OXYGEN DELIVERY BY OUTGASSING OF HYPERBARICALLY LOADED MICROTANKS AND BULK POLYMERS FOR BIOMEDICAL APPLICATIONS

by
Colin Andrew Cook

A thesis submitted to Johns Hopkins University in conformity with
the requirements for the degree of Master of Science in Engineering

Baltimore, Maryland, USA
August, 2014

© 2014 Colin Andrew Cook
All Rights Reserved

ABSTRACT

Oxygen diffusion limitations within nascent tissue engineering scaffolds leads to the development of hypoxic regions, cell death, and graft failure. Diffusion limitations are most severe in scaling from the mm-sized grafts studied in rodents to the cm-sized grafts required for human patients and thus represent a major barrier to clinical translation. Extensive efforts have been made to delivery oxygen within tissue engineering scaffolds to help maintain cell viability during the period of vascular development and anastomosis. Unfortunately, the approaches that have been developed which include peroxide-doping, perfluorocarbons, hyperbaric oxygen therapy have lacked cytocompatability, oxygen capacity, and practicality, respectively. The outgassing of oxygen from hyperbarically loaded polymers represents a novel and elegant solution that addresses these shortcomings. Many commonly used biocompatible polymers possess high resistance to oxygen diffusion but a non-trivial solubility of oxygen (on the order of 10% V/V/atm). Thus it is possible to load the polymer with oxygen gas using a hyperbaric chamber and to subsequently achieve a prolonged delivery of oxygen as the polymer outgasses. By forming microscopic polymeric shells with a hollow core, the loading efficiency of oxygen can be greatly enhanced and such a structure is termed a *microtank*. In this thesis, we will describe the development and empirical validation of the theory governing the oxygen delivery from hyperbarically loaded materials, including microtanks. Oxygen loaded microtanks and/or bulk polymers can be combined with a hydrogel phase to form a scaffold with oxygen delivery throughout. This oxygen delivery approach has been shown to enhance the survival of human cells cultured under anoxic conditions for out to 6 days. Beyond tissue engineering, hyperbaric oxygen loading could

be used to functionalize many clinically used polymer implants such as screws, suture anchors, stiches, etc. as elevated local oxygen tensions have been shown to enhance collagen deposition and reduce infection. Indeed, the biomedical applications are diverse and abundant.

Faculty Readers:

Dr. Warren Grayson (advisor), Dr. Jordan Green, and Dr. Hai-Quan Mao

PREFACE

This dissertation is original, independent work by the author, C.A. Cook.

DEDICATION

This work is dedicated to my parents Ainslie and Andrew Cook, my maternal grandparents Gwenneth and Wilfred Goodman, my paternal grandparents Iris and Ken Cook, my siblings Sandra, Olivia, and Elaine Cook, my aunts, uncles and cousins, and my friend Maximillian Klas. You have shown me the power of an individual to change the world. You have opened my eyes to the goodness of humanity. You have focused my energy and purpose on causes worthwhile. Each of you is a source of strength, wisdom, and encouragement. Be gone with superstition!

ACKNOWLEDEMENTS

Many thanks to my advisor Dr Warren Grayson for his support, guidance, and encouragement with this endeavor. Thank you to the other faculty of the Translational Tissue Engineering Center, Drs. Elisseeff, Green, Mao, and Yarema, for creating a supportive, collaborative, and enterprising organization in which I could grow as an engineering scientist. To my Hopkins friends and colleagues, your enthusiasm and passion for science, life, and the betterment of humanity is laudable. To Jay Burns, thank you for your wizardry and patience in the machine shop. To the broader BME faculty, and notably Professor Tza-Huei Wang, you set a high bar in teaching excellence. I have very much enjoyed my time as a member of the Johns Hopkins community!

TABLE OF CONTENTS

CHAPTER I: Biological Requirements for Oxygen within Tissue Engineering ... 1

Mass transport within tissue engineered grafts ... 1

3D Finite Difference Models of Nutrient Transport within Grafts ... 4

Defining Normoxia, Hypoxia, Hyperoxia, and Anoxia ... 7

Cell and Tissue Level Response to Hypoxia ... 9

Pathologies Caused by Hypoxia ... 10

Survey of Oxygen Delivery Technologies ... 11

Biological and medical consequences of hyperoxia ... 14

CHAPTER II: Theory of Oxygen Delivery Hyperbarically Loaded Materials ... 16

Diversity of Polymer Properties ... 16

Polymer Gas Barriers ... 17

Outgassing of a polymer slab ... 21

Temperature Dependence of Permeation ... 24

Outgassing of a hollow polymeric shell ... 26

Mechanical Considerations ... 32

Conception of Microtanks and Microtank-loaded Scaffolds ... 33

Outgassing from Composites of Microtanks Suspended in Bulk Polymer ... 35

CHAPTER III: Oxygen Delivery from Hyperbarically Loaded MicroTanks Extends Cell Viability in Hypoxic Environments ... 36

Manuscript for Publication ... 36

Hyperbaric Chamber Apparatus ... 36

INTRODUCTION ... 38

MATERIALS & METHODS ... 41

Fabrication of Microtank Containing Scaffolds ... 41

Loading of Microtank Containing Disks ... 41

Quantitative Measurement of Oxygen Release Profiles ... 41

Visualization and Semi-quantitative Measurement of Oxygen Release ... 42

Cell Culture and Media Conditions ... 43

Vascular Assembly ... 45

PicoGreen DNA Assay ... 45

Alamar Blue Assay 45
Predictions of Cellular Oxygen Uptake Rates 46
RESULTS 47
Governing Equations of Oxygen Delivery from Microtank Containing Scaffolds 47
Colorimetric Assay of Oxygen Delivery 49
Tuning Oxygen Delivery Profiles 49
Scaffold Storage 50
Time course of Therapeutic Effect 51
Sensitivity to Oxygen Delivery vs Cellular Demand 52
Oxygen Delivery Enhances Vessel Formation 53
DISCUSSION 54
CONCLUSION 57
FIGURES 58
CHAPTER IV: Translational Efforts and Applications 63
Development of standalone microtanks 63
Double emulsion approaches to engineer standalone microtanks 63
Results: 65
Interfacial polymerization approach, new chemistries, results 67
Simplicity by thoughtful reduction – Outgassing of polymeric foams 70
Product design and applications 72
Potential Synergy with Dimethyloxaloylglycine HIF-1α 73
CHAPTER V: Commercialization and Translation Strategy 74
Defining Target Markets 74
Medical Fasteners 75
Suture Anchors 77
Other Applications 78
Entry Strategy into Medical Fasteners 79
Wound Care & Graft Management 81
Entry Strategy into Wound Care 83
Intellectual Property Protection 84
REFERENCES 85

LIST OF FIGURES

FIGURE I-1: THIELE MODULUS INDICATES OXYGEN DIFFUSION LIMITATIONS WITHIN TISSUE ENGINEERED SCAFFOLDS. (A) THIELE MODULUS AS A FUNCTION OF CELL CONCENTRATION AND SCAFFOLD THICKNESS, H. (B) SCAFFOLDS OF IDENTICAL THIELE MODULI ILLUSTRATING RELATIONSHIP BETWEEN CELL CONCENTRATION AND SCAFFOLD THICKNESS. REPRODUCED FROM EHSAN, S. ET AL., 2013.[9] _____ 2

FIGURE I-2: THREE DIMENSIONAL FINITE DIFFERENCE MODELING INDICATES RAPID ONSET OF HYPOXIA. TIME COURSE OF OXYGEN TENSION AT CENTRAL SLICE WITHIN CELLULARIZED (5×10^6 CELLS/ML) FIBRIN GEL (1CM,1CM,3CM) AS CALCULATED BY FINITE DIFFERENCE MODELING. GEL IS DEMARCATED BY THE DASHED LINE AND BOUNDARIES ARE HELD AT 140MMHG. STEADY STATE REACHED BY APPROXIMATELY 12HRS. OXYGEN TENSIONS ARE REPRESENTED COLORIMETRICALLY FROM 140MMHG (20%) TO 0MMHG (0%) AS INDICATED BY THE LEGEND. _____ 6

FIGURE I-3: OXYGEN DIFFUSION LIMITATIONS BECOME SIGNIFICANT IN CM-SCALE SCAFFOLD. PLOTS OF CENTRAL OXYGEN TENSION OVER TIME IN [3,3,1CM] (BLUE) VS [3,3,1MM] (RED) CELLULARIZED (5×10^6 CELLS/ML) FIBRIN GEL, HIGHLIGHTING A MAJOR BARRIER TO CLINICAL TRANSLATION. SIZE SCALES AND THE CELL SEEDING DENSITY ARE REPRESENTATIVE OF A TISSUE-ENGINEERED GRAFT FOR A HUMAN/PORCINE AND RODENT, RESPECTIVELY. INSET IMAGE DEPICTS A GRAFT OF THE ANGLE OF THE MANDIBLE FOR A PIG COMPARED TO A RAT. _____ 7

FIGURE II-1: GAS TRANSPORT THROUGH A POLYMER SLAB INVOLVES ADSORPTION, DIFFUSION, AND DESORPTION. GAS DISSOLVES INTO THE POLYMER AT THE SURFACES ACCORDING TO HENRY'S LAW. IF A PRESSURE DIFFERENTIAL IS INDUCED ACROSS THE SLAB, THEN THE CONCENTRATION OF DISSOLVED GAS PARTICLES WILL BE HIGHER ON THE HIGH-PRESSURE SIDE. THIS CONCENTRATION GRADIENT WILL DRIVE THE DIFFUSION OF PARTICLES THROUGH THE POLYMER TO THE LOW-PRESSURE SIDE WHERE THEY WILL EXIT BY DESORPTION. MODIFIED FROM FOOD PACKAGING PERMEABILITY BEHAVIOUR: A REPORT[55]. _____19

FIGURE II-2: GEOMETRICAL CONSIDERATIONS OF OXYGEN OUTGASSING FROM A HOLLOW POLYMERIC SHELL OR MICROTANK. A MICROTANK COMMONLY HAS A SPHERICAL GEOMETRY WITH RADIUS R, A SHELL THICKNESS D, AND IS COMPOSED OF A POLYMER WITH A PERMEABILITY Σ. MICROTANKS ARE COMMONLY ON THE ORDER OF 100MM IN DIAMETER WITH A SHELL THICKNESS OF 1-10MM. _____27

FIGURE II-3: FREE BODY DIAGRAM OF A SPHERICAL THIN-WALLED PRESSURE VESSEL. (LEFT) IN THE MECHANICAL ANALYSIS, A CENTRAL SLICE IS MADE THROUGH THE PRESSURE VESSEL. (RIGHT) THE PRESSURE P ACTING ON THE CROSS SECTIONAL AREA OF THE CORE GENERATES A FORCE P×A THAT MUST BE BALANCED BY TENSILE STRESSES Σ IN THE SHELL. _____32

FIGURE III-1: A HYPERBARIC CHAMBER IS USED TO LOAD SCAFFOLDS AND MICROTANKS WITH OXYGEN. (A) COMSOL FEM MODELING WAS USED TO ENSURE A FACTOR OF SAFETY OF 3 WHILE OPERATING WITHIN THE DESIGN LIMIT OF 100ATM. (B) VALVE LAYOUT OF HYPERBARIC CHAMBER: BLEED VALVE ALLOWS DEPRESSURIZATION, PRESSURE GAUGE PROVIDES PRESSURE READOUT, PRESSURE RELIEF VALVE PROVIDES PROTECTION AGAINST

over-pressurization, and quick connect valve allows for easy attachment to the high pressure regulator and oxygen tank. (C) View of assembled hyperbaric chamber. (D) Side view of lid, Teflon O-ring gap, and base, with high tensile strength bolts. (E) 2.5-inch diameter by 2-inch deep chamber fits a pig mandibular scaffold. ____ 37

Figure III-2: Schematic of microtank loaded PCL scaffolds. Scaffolding material composed of PCL is embedded with microtanks to create a syntactic foam with distributed closed-cells. The microtanks contain a hollow core, which can be hyperbarically loaded with gaseous oxygen, surrounded by a polymeric shell composed of a structural, oxygen barrier layer to contain the pressurized oxygen. The pressure differential across the microtank shell drives the outward diffusion of oxygen through the shell and into the bulk PCL where it continues to diffuse out to the periphery of the scaffolding and into the media/hydrogel to nourish cells. The release of oxygen from microtank embedded scaffolds is regulated by the rate of permeation through the shell plus the rate of permeation through the bulk phase. ____ 58

Figure III-3: Microtanks enhance oxygen delivery capacity and duration. (A) Oxygen delivery from hyperbarically loaded disks with microtanks (+uTanks) compared to without (-uTanks), fitted with theoretical delivery profile to extract time constants of delivery. (B) Total oxygen delivered was calculated by integrating the delivery curves while time constants of delivery were calculated from fit. ____ 59

Figure III-4: Resazurin assay provides colorimetric visualization and quantitation of oxygen delivery duration from microtank containing PCL disks. (A) Photograph of 2mm thick disks in resazurin solution indicating oxygen release (pink) over a period of 2 days. (B) Green channel of photographs (left) are used to quantify the thickness of the resazurin bands emanating from the disks by plotting the average horizontal profile of the image (green box) and extracting the band widths (red) and disk thickness (blue) at half maximum. (C) Plotting the thickness of the resazurin band over time (blue circles) and fitting with the theoretical oxygen delivery equation (red) allows for the extraction of the time constant of delivery. ____ 59

Figure III-5: Time constant of oxygen delivery increases with polymer thickness. Stacked bar graphs illustrate the contribution of the microtank (blue) vs bulk phase (red) time constants to the total outgassing time constant. Microtank filled PCL disk with thicknesses of 1mm, 2mm, and 4mm (pictured below in resazurin solution) were monitored over 1 week to extract time constants of delivery (above). N=3. * indicates significant difference ($P<0.05$ by one-way ANOVA and Tukey's HSD). ____ 60

Figure III-6: Amount of oxygen delivery increases with microtank concentration. Plot of relative amount of oxygen released at 1hr time point from PCL disks containing 0, 1.4, or 7% V/V microtanks, normalized to pure PCL disk. N=3. * indicates significant difference ($P<0.05$ by one-way ANOVA and Tukey's HSD) between the 7% and the 0%, 1.4% groups. ____ 60

FIGURE III-7: LOW TEMPERATURES ENABLE STORAGE OF HYPERBARICALLY LOADED SCAFFOLDS. PLOT OF RELATIVE AMOUNT OF OXYGEN DELIVERED AT 1 HR TIME POINT FROM HYPERBARICALLY LOADED PCL DISKS CONTAINING MICROTANKS THAT WERE STORED FOR 1 WEEK IN AMBIENT PRESSURE AT 20°C, -20°C, OR -80°C, NORMALIZED TO DISKS STORED UNDER LOADING CONDITIONS IN HYPERBARIC CHAMBER. (N=2). * INDICATES SIGNIFICANT DIFFERENCE ($P<0.05$ BY ONE-WAY ANOVA AND TUKEY'S HSD) FROM ALL OTHER GROUPS. _____61

FIGURE III-8: TIME COURSE OF ASC METABOLISM UNDER ANOXIC CONDITIONS. RESULTS OF ALAMAR BLUE ASSAY OF ASCS CULTURED IN 3D FIBRIN GELS ON TOP OF PCL DISKS CONTAINING OXYGEN LOADED MICROTANKS (UTANKS), NITROGEN PURGED MICROTANKS (NEG), OR AMBIENT MICROTANKS (POS). UTANK AND NEG GROUPS WERE CULTURED UNDER ANOXIA (0% O_2, 5% CO_2, 95% N_2) WHILE THE POS GROUP WAS CULTURED UNDER NORMOXIA (21% O_2, 5% CO_2, 74% N_2). N=3. * INDICATES SIGNIFICANT DIFFERENCE ($P<0.05$ BY ONE-WAY ANOVA AND TUKEY'S HSD) BETWEEN INDICATED PAIRS. _____61

FIGURE III-9: AMOUNT OF OXYGEN DELIVERY INFLUENCES CELLULAR GROWTH. (A) THEORETICAL RATIO OF OXYGEN DELIVERY FROM MICROTANK LOADED PCL DISKS TO CELLULAR DEMAND OVER 6 DAY CULTURE BASED ON INITIAL CELL NUMBER, OXYGEN UPTAKE RATES FROM THE LITERATURE, AND MEASURED DELIVERY PROFILES. DISKS WERE LOADED WITH OXYGEN UNDER THE SAME CONDITIONS AND PRE-RELEASED FOR 3, 2, OR 1 DAYS BEFORE CELL ENCAPSULATION IN GEL TO ACHIEVE THE HIGH, MEDIUM, AND LOW DELIVERY PROFILES. DASHED LINE INDICATES THRESHOLD WHERE DELIVERY IS EQUAL TO DEMAND. (B) CHANGE IN DNA CONTENT BY PICOGREEN ASSAY WITHIN GELS BETWEEN DAY 0 AND 6 DAYS OF ANOXIC CULTURE (NEG, HIGH, MED, LOW) OR NORMOXIC CULTURE (POS). BLACK LINE INDICATES AVERAGE GROWTH IN GROUPS THAT RECEIVED BI-DAILY FEEDINGS (DASHED LINES REPRESENT CORRESPONDING STANDARD DEVIATION); ALL OTHER GROUPS RECEIVED ONLY AN INITIAL 5ML OF MEDIA. (N=4). ALL DIFFERENCES ARE STATISTICALLY SIGNIFICANT ($P<0.05$ BY ONE-WAY ANOVA AND TUKEY'S HSD), EXCEPT POS VS MED AND NEG VS DAY 0 AS INDICATED BY N.S. _____62

FIGURE III-10: MICROTANKS ENHANCE VESSEL FORMATION UNDER ANOXIC CONDITIONS. (A) CONFOCAL LIVE (GREEN) /DEAD (RED) IMAGES (5X) OF ASC:HUVECS IN FIBRIN GELS AT DAY 4. REPRESENTATIVE IMAGES SHOWN N=4. (B) QUANTIFICATION OF IMAGES USING THE RATIO OF AREAS OF LIVE AND DEAD CELLS. * INDICATES SIGNIFICANT DIFFERENCE BY STUDENT'S T-TEST ($P<0.05$). _____62

FIGURE IV-1: BRIGHT FIELD IMAGES OF PLGA/PVA MICROTANKS FORMED BY DOUBLE EMULSION. (A, B) CORE-SHELL MORPHOLOGY IS APPARENT IN MANY PARTICLES (C) PARTICLES DEVELOP A DARKER COLORED SHELL SURROUNDING THE CORE FOLLOWING VACUUM DRYING, INDICATING DEPOSITION OF PVA AROUND THE INTERIOR SURFACE (D, E) PVA MICROTANKS ARE OBSERVED FLOATING INDICATING THEY ARE INDEED HOLLOW. APPROXIMATELY SPHERICAL GEOMETRIES ARE OBTAINED WITH SOME VISIBLE IMPERFECTIONS (F, G) PVA PARTICLE ILLUSTRATING HOLLOW CORE AND SUBSEQUENT MANIPULATION ON A NEEDLE TIP. _____66

FIGURE IV-2: CAPILLARY MICROFLUIDIC APPROACH TO CORE-SHELL PARTICLE FORMATION. THE INNER PHASE IS INJECTED THROUGH A CONCENTRIC NEEDLE INTO THE MIDDLE PHASE. THESE CONCENTRIC STREAMS ARE SUBSEQUENTLY ENCAPSULATED BY THE OUTER PHASE AND BREAK UP INTO DROPLETS WITH A CORE-SHELL MORPHOLOGY. VARYING THE RESPECTIVE FLOW RATES CAN ALTER THE PARTICLE GEOMETRY AND RELATIVE PROPORTIONS OF THE SHELL AND CORE. REPRODUCED FROM SHUM, H. C. ET AL., 2008[66]. _____67

FIGURE IV-3: INTERFACIAL POLYMERIZATION APPROACH YIELDS MONOCORE PVA FILLED MICROCAPSULE. (A) A SINGLE EMULSION IS FORMED WITH EACH PHASE CONTAINING A MONOMER REACTIVE WITH THE COMPLIMENTARY MONOMER IN THE OPPOSITE PHASE. AT THE INTERFACE WHERE THE MONOMERS ARE ABLE TO MEET, A URETHANE LINKAGE FORMING REACTION OCCURS PRODUCING A POLYMERIC SHELL THAT ENCAPSULATES THE DISPERSED PHASE. (B) BRIGHT FIELD MICROSCOPE IMAGES OF PVA FILLED MICROCAPSULES PRODUCED USING THIS METHOD. 69

FIGURE IV-4: EXISTING MEDICAL APPLICATIONS MAY BENEFIT FROM HYPERBARIC OXYGEN LOADING AND DELIVERY. (A) SPINAL FUSION CAGES (B) SUTURE ANCHORS (C) MEDICAL FASTENERS AND SCREWS (D) PEEK IMPLANTS 73

FIGURE V-1: PATHWAYS FROM TECHNOLOGY TO MARKETS. SOLID LINES INDICATE TECHNOLOGY / MARKETS THAT EXIST TODAY WHERE AS DASHED LINES INDICATE TECHNOLOGY / MARKETS IN DEVELOPMENT. MEDICAL FASTENERS AND WOUND CARE REPRESENT THE MOST IMMEDIATE MARKETS TO TARGET. 75

FIGURE V-2: OXYGEN DELIVERY PERIODS OF COMMONLY USED MEDICAL POLYMERS. THE TIME CONSTANT OF OXYGEN DELIVERY FROM AN EXISTING MEDICAL FASTENER, IMPLANT, OR DEVICE CAN BE EASILY ESTIMATED FROM THIS CHART IF THE POLYMER AND CHARACTERISTIC THICKNESS ARE KNOWN. 77

FIGURE V-3: SMITH AND NEPHEW PEEK POLYMER SUTURE ANCHORS. (L-R) RAPTORMITE, DYNOMITE, SPYROMITE MODELS. DIAMETERS ARE 3MM, 2MM, 2MM, RESPECTIVELY. 78

LIST OF TABLES

TABLE 1: TABLE OF OXYGEN PERMEABILITY VALUES OF COMMONLY USED PACKAGING MATERIALS. (*P) INDICATED THE PERMEABILITY OF THE FILMS IN UNITS OF CM^3.20UM/M^2.DAY.ATM AT A TEMPERATURE OF T IN KELVIN (K=273+°C). REPRODUCED FROM KURARAY EVAL EVOH RESINS BROCHURE[56]. THE PERMEABILITY OF A POLYMER IS A HIGHLY TEMPERATURE DEPENDENT PROPERTY, ROUGHLY DOUBLING WITH A 10°C INCREASE IN TEMPERATURE.....20

This page is intentionally left blank.

CHAPTER I:

Biological Requirements for Oxygen within Tissue Engineering

Mass transport within tissue engineered grafts

Tissue engineered bone, muscle, liver, fat, and blood vessels have all been successfully demonstrated in small animal models. These successes are a bellwether of the promise of regenerative medicine to revolutionize healthcare by providing patient-specific grafts to replace damaged or failing tissue. These reports have helped elucidate the underlying mechanisms governing tissue formation and provided encouraging proofs-of-concept; however, they often overlook the challenges[1–4] associated with scaling the grafts from the mm^3 domain of mice and rats to the cm^3 domain of humans.

Within small grafts the process of diffusion alone can accommodate the transport of nutrients, oxygen, and waste, where as in larger, diffusion-limited grafts, convection is required to meet metabolic needs. Unfortunately, convection requires functional vascular networks[5,6] and these can take several days to weeks to form. During this period, cellular metabolic demand exceeds supply leading to nutrient deficiency and hypoxia[1,7,8], which can ultimately result in cell death and graft failure if persistent.

Diffusion limitations apply to all metabolic molecules and can be estimated by comparing rates of delivery and/or generation to rates of consumption, as is captured in the Thiele modulus[9] (1D case):

$$\phi = h\sqrt{\frac{\rho_{cell} V_{max}}{K_m D}}$$

(I-1)

With scaffold thickness h, cell density ρ_{cell}, cellular oxygen uptake rate V_{max}, Michaelis constant K_m, and oxygen diffusion constant D. A large Thiele modulus indicates diffusion limitations and hence the presence of gradients. Figure I-1[9] illustrates how scaffold thickness and cellularity affect the Thiele modulus, reproduced from Ebsan, S. et al., 2013.

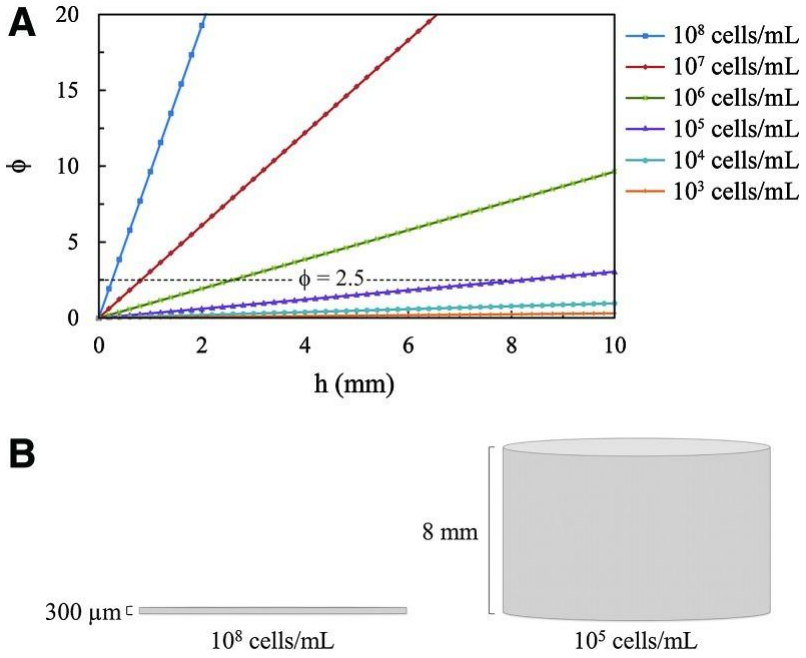

Figure I-1: Thiele modulus indicates oxygen diffusion limitations within tissue engineered scaffolds. (A) Thiele modulus as a function of cell concentration and scaffold thickness, h. (B) Scaffolds of identical Thiele moduli illustrating relationship between cell concentration and scaffold thickness. Reproduced from Ehsan, S. et al., 2013.[9]

When considering cell metabolism both the deficit of nutrients as well as the accumulation of waste products can be problematic[10,11]. However, in examining the equations governing glucose metabolism, the importance of oxygen is highlighted.

Aerobic Metabolism of Glucose:

$$C_6H_{12}O_6 + 6O_6 \rightarrow 6CO_2 + 6H_2O + \sim 30ATP$$

(I-2)

Anaerobic Metabolism of Glucose:

$$C_6H_{12}O_6 \rightarrow 2CH_3CH(OH)COOH + 2ATP$$

(I-3)

If oxygen is present, cellular respiration is able net around 30 ATP per glucose molecule and the relatively fast-diffusing CO_2 waste product. If oxygen is not available anaerobic glycolysis is only able to net 2 ATP plus the relatively slow-diffusing lactic acid waste product[7,12]. From the perspective of the Thiele modulus, if the energy requirements of the cell are to be maintained then the consumption of glucose under anaerobic conditions, $V_{max,\ anaerobic}$, needs to be $15 \times V_{max,\ aerobic}$. Thus the Thiele modulus of glucose under anaerobic conditions is $\sqrt{15} \times \approx 4 \times$ that of aerobic conditions, so diffusion-limitations occur over proportionally shorter

distances. This is in addition to the more diffusion-limited and less tolerated waste product lactic acid.

3D Finite Difference Models of Nutrient Transport within Grafts

In order to understand more precisely the scales at which diffusion limitations become important, a computational model of cellular metabolism and diffusional mass transport was created. The model employs the finite difference method to solve Fick's laws of diffusion over the scaffold geometry with consideration for local cell density, oxygen uptake rate, and diffusion constants. A Michaelis-Menten type model was used to predict the cellular oxygen uptake rate with parameters obtained from the literature[9]. A square slab geometry was predominantly used with length scales varying from mm to cm to model tissue dimensions up to clinically relevant sizes. Typical cell seeding densities for tissue engineering constructs were used. The parameters of the model were varied during sensitivity analysis, but representative values are as follows:

Diffusion of Oxygen in Hydrogel: $D_{O2} = 1.7\times10^{-9}$

Cellular Oxygen Uptake Rate: $V_{max} = 1.3\times10^{-17}$ mol/cell/s

Oxygen Concentration at Half-Maximum OUR: $K_m = 5.6$ mmHg

Oxygen Solubility in Hydrogel: $S_{O2} = 1.19\times10^{-6}$ mol/L/mmHg

Boundary Condition of Oxygen Concentration: $C_{O2,\infty} = 140$ mmHg

Cellular Density within Hydrogel: $\rho_{cell} = 5\times10^{6}$ cells/mL

Michaelis-Menten Equation for Volumetric Oxygen Uptake Rate (OUR):

$$OUR = \rho_{cell} V_{max} \frac{C_{O_2}}{K_m + C_{O_2}} \quad \textbf{(I-4)}$$

Fick's Second Law of Diffusion:

$$\frac{\partial C_{O_2}}{\partial t} = D\left(\frac{\partial^2 C_{O_2}}{\partial x^2} + \frac{\partial^2 C_{O_2}}{\partial y^2} + \frac{\partial^2 C_{O_2}}{\partial z^2}\right) \quad \textbf{(I-5)}$$

Space and time discretized as:

$$\Delta C_{x,y,z}^{t+\Delta t} = \left\{ D \sum_{j=x,y,z} \left[\frac{C_{j+\Delta j}^t + C_{j-\Delta j}^t - 2C_j^t}{(\Delta j)^2}\right] - \rho_{cell} V_{max} \frac{C_j^t}{K_m + C_j^t} \right\} \Delta t \quad \textbf{(I-6)}$$

The results of the simulation with the aforementioned conditions, illustrated how quickly and to what extent diffusion limitations affect tissue engineered grafts. Figure I-2 depicts the oxygen concentrations through the central slice of a 3cm×3cm×1cm hydrogel over a period of 12 hours. Of note, is the rate at which hypoxia develops within cm-sized grafts and the relative size of the hypoxic region, with oxygen tension dropping below 1% after only 3hrs. Given the strong

dependence of cell function, differentiation, and proliferation on oxygen tension it would be virtually impossible to achieve a desired outcome with such strong gradients.

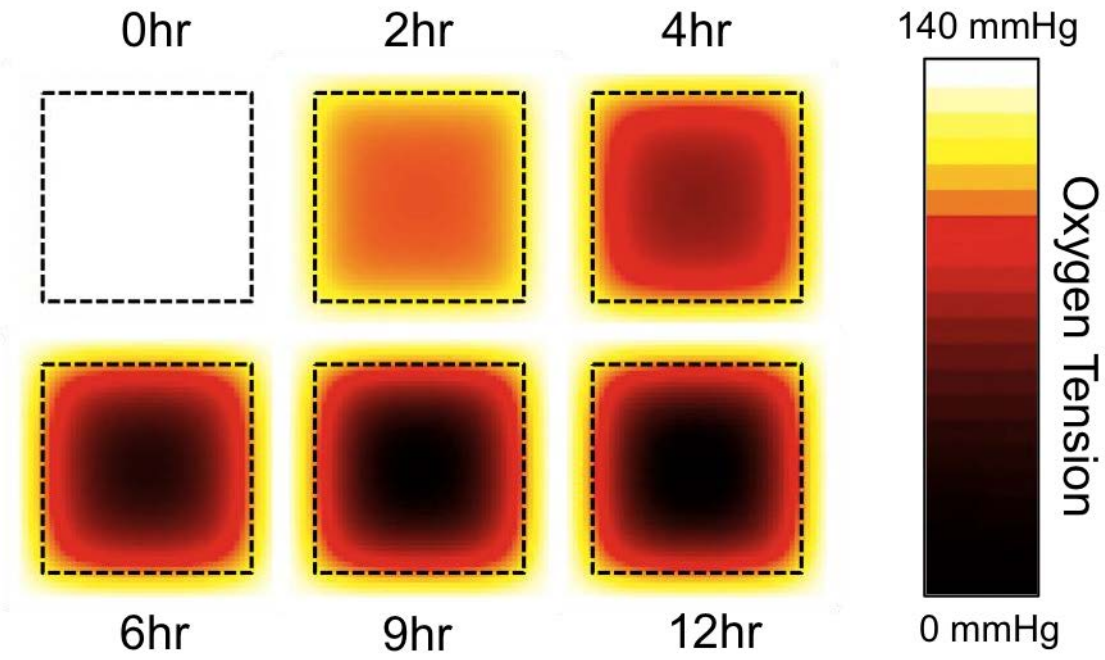

Figure I-2: Three dimensional finite difference modeling indicates rapid onset of hypoxia. Time course of oxygen tension at central slice within cellularized (5×10^6 cells/mL) fibrin gel (1cm,1cm,3cm) as calculated by finite difference modeling. Gel is demarcated by the dashed line and boundaries are held at 140mmHg. Steady state reached by approximately 12hrs. Oxygen tensions are represented colorimetrically from 140mmHg (20%) to 0mmHg (0%) as indicated by the legend.

Additionally, the model was run for different size scales to investigate the effect of scaffold size on oxygen tension within the grafts. Figure I-3 presents the plots of oxygen tension at the center of each scaffold: 3mm×3mm×1mm versus 3cm×3cm×1cm, representative of scaling between a mouse and a human. The results indicate that gradients do not significantly affect mm-scale scaffolds but do

greatly affect cm-scale scaffolds. Therefore, for the clinical translation of tissue engineered grafts it will be necessary to address oxygen diffusion limitations.

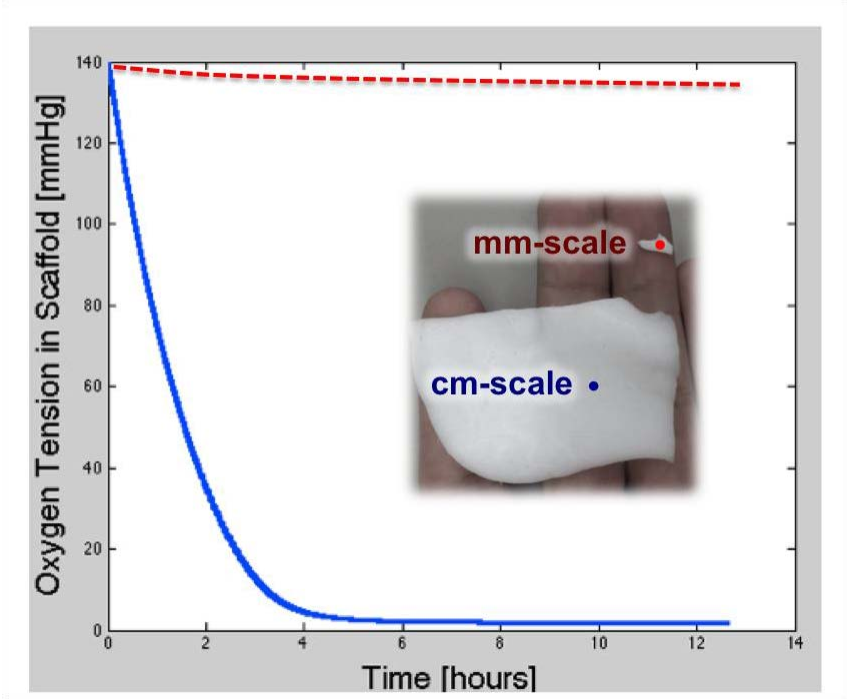

Figure I-3: Oxygen diffusion limitations become significant in cm-scale scaffold. Plots of central oxygen tension over time in [3,3,1cm] (blue) vs [3,3,1mm] (red) cellularized (5×10^6 cells/mL) fibrin gel, highlighting a major barrier to clinical translation. Size scales and the cell seeding density are representative of a tissue-engineered graft for a human/porcine and rodent, respectively. Inset image depicts a graft of the angle of the mandible for a pig compared to a rat.

Defining Normoxia, Hypoxia, Hyperoxia, and Anoxia

The terms referring to oxygen concentrations have been used ambiguously within the literature depending on whether one is referring to in vivo or ex vivo microenvironments. By convention, within ex vivo culture the terms normoxia refers to 20% O_2 where as in vivo the term normoxia usually refers to a range of 2-8% O_2. Furthermore, different cell types have different tolerances for hypoxic

conditions: a bone-marrow derived mesenchymal stem cell might be happy at an oxygen tension of 13mmHg (1.8%)[13] where as a cardiomyocyte would find such an environment detrimental, preferring something around 46mmHg (6%)[14].

Within this document the amount of oxygen supplied compared to the estimates of cellular demand will be provided where possible. Where references are made to normoxia, hypoxia, hyperoxia, and anoxia the following definitions will be observed to remain consistent with the field of tissue engineering:

Normoxia – Normal oxygen levels. In reference to ex vivo culture, 20% O_2. In reference to in vivo contexts, 2-8% O_2.

Hypoxia – Deficient oxygen levels. In reference to ex vivo culture, below 20% O_2; most hypoxia experiments are conducted between 1-5%O_2. In reference to in vivo contexts, typically below 2% O_2.

Hyperoxia – Excessive oxygen levels. In reference to ex vivo culture, greater than 20% O_2. In reference to in vivo contexts, greater than 8% O_2.

Anoxia – Absence of oxygen. In reference to ex vivo culture or in vivo culture, 0% O_2.

Cell and Tissue Level Response to Hypoxia

Oxygen is clearly an important molecule for the metabolic function of the mammalian cell, and beyond this role it functions as a potent modulator of cell function and wound repair[6]. Hypoxic environments can have divergent effects on cells depending on whether the exposure is acute or chronic. Increased production of specific extracellular matrix proteins and enhanced angiogenesis are observed effects of acute hypoxic exposure, while reduced cellular respiration and proliferation are observed under chronic exposure. Oxygen tension has also been shown to direct cell fate.

Cellular responses to hypoxia are primarily mediated through the hypoxia inducible factor pathway[15], although there are non-HIF mediated responses. Briefly, the pathway is composed of two transcription factors: HIF-1α, which contains an oxygen-dependent degradation domain that leads to degradation under normoxic conditions, and HIF-1β, which is constitutively expressed and dimerizes with available HIF-1α to form a basic helix-loop-helix transcription factor that can bind to hypoxia-responsive elements to drive gene expression. Thus, when the cell experiences hypoxia, the degradation of HIF-1α slows, leading to build up of HIF-1α within the cell to drive signaling. Hypoxia-responsive elements have been found to drive a large number of metabolic, vascular, and survival genes, including: glucose transporter 1, enolase 1, erythropoietin, VEGF, and p21[10].

Local oxygen concentrations have been demonstrated to direct cellular differentiation, notably in bone and cartilage where hypoxia favors the formation of cartilage. For example, primary rat osteoblasts[16] and human bone marrow derived

stem cells[17] cultured under hypoxic conditions were inhibited from differentiating down to an osteogenic phenotype. Similarly, a study[18] that cultured cells from the embryonic chick tibial cortex under 35% vs 5% O_2 found differentiation towards bone under high levels of oxygen and cartilage under low levels. While the use of oxygen tension to direct cell fate may be possible, it is exceedingly difficult in practice due to the steep gradients that develop within grafts.

Within wound healing, acute hypoxia caused by the disruption of local vasculature plays an important role during angiogenesis[19–21] by inducing expression of cytokines, growth factors (e.g. PGDF, VEGF, TGF- β), and matrix molecules through the HIF pathway. In addition to hypoxia, HIF-1α has been shown[22] to be stimulated by pro-inflammatory factors like interleukin-1 shortly after injury. However, chronic exposure to hypoxia has been shown to reduce the capacity for wound healing processes[23] resulting in chronic wounds and sores.

Pathologies Caused by Hypoxia

Within tissue engineering, the failure of large grafts is routinely tied to the formation of a chronic hypoxic core, which eventually leads to necrosis. Beyond tissue engineering hypoxia is indicated in the etiology of a number of pathologies including: diabetic ulcers and chronic wounds, renal disease, graft necrosis, gangrene, myocardial infarction, cerebrovascular insult, tumors, infections, among others. The loss of vasculature perfusion, either by slow regression of the network, surgical dissection, or occlusion, prevents cells from receiving adequate oxygen and they eventually undergo necrosis. Hypoxia can also lead to compromised ECM

production, altered metabolism, reduced nitric oxide production, and increased MMP production[24]. Tissues within a hypoxic state are particularly susceptible to infection by opportunistic bacteria due to the suppressed activity of the immune system, particularly the respiratory burst response of leukocytes, as it is dependent on the conversion of local oxygen to H_2O_2 and hypochlorite[25,26].

Survey of Oxygen Delivery Technologies

Given the deleterious consequences of hypoxia within diffusion-limited grafts and pathologies, a number of approaches have been investigated to augment oxygen supply to maintain cell viability during the period of vascularization and promote healing. These have included: hyperbaric oxygen therapy where the patient and/or graft is placed in an oxygen enriched environment to enhance the oxygen content dissolved in the blood and interstitial fluid[24,27–29], perfluorocarbon emulsions which utilize the high oxygen solubility properties of these chemicals to enhance diffusion rates[2,30–33], and various peroxide compounds which generate oxygen during a decomposition reaction[34–36]. While each of these approaches has highlighted the benefits of oxygen augmentation, they unfortunately each suffer from limitations in terms safety and/or efficacy that have prevented their widespread adoption. The following section will explore these approaches in further detail and evaluate their advantages, disadvantages, and limitations.

Hyperbaric oxygen therapy (**HBO**) is the oldest and most clinically relevant approach available. It involves placing the patient within an oxygen-enriched environment for an extended period of time, commonly under hyperbaric

conditions (typically, 30-90min, 100% O_2, 2.5atm)[24], with the aim of increasing the oxygen content within the blood and thus increasing the delivery of oxygen to cells. HBO is indicated for the following conditions[37]: air or gas embolism, carbon monoxide poisoning, clostridial myositis (gas gangrene), crush injury, compartment syndrome and other acute traumatic ischemias, decompression sickness, enhancement of healing in selected problem wounds, exceptional blood loss (anemia), intra-cranial abscess, necrotizing soft tissue infections, osteomyelitis (refractory), delayed radiation injury (soft tissue and bone), skin grafts and flaps (compromised), and thermal burns. Of note is that virtually all of these conditions have existing blood vessels through which the oxygen-enriched blood can reach the target area. The approach may double or quadruple the effective diffusion distance away from capillaries, but this is of little use for avascular grafts. However, HBO has been shown to increase vascularization[28], partly through the release of endothelial progenitor cells from the bone marrow, and improve tissue healing so it may play an adjunctive role to help with the engraftment post-implantation. The greatest limitation with HBO is that it requires frequent visits to a clinical center, it is an intermittent therapy, and it must be administered systemically.

Perfluorocarbons are a class of highly fluorinated hydrocarbons liquids with a unique capacity for dissolving gases, commonly between 35-55% V/V[38] for oxygen. They are biologically inert and neither hydrophobic nor hydrophilic due to uniquely low intermolecular attractive forces. They are commonly delivered as an emulsion into the blood stream with two primary therapeutic effects: firstly, they increase the capacity for dissolved oxygen within the blood, and secondly they increase the

effective diffusion distance of oxygen by facilitating transport. Unfortunately, in many pathologies the reloading of the emulsion as it passes through the lungs is negligible. The same can be said within tissue engineering applications where oxygen loaded perfluorocarbons contribute only an initial burst of oxygen to the graft. The utility of perfluorocarbon emulsions is thus primarily attributable to their ability to increase the plasma diffusivity of oxygen, upwards of 10 to 50-fold[39], although the actual mass movement of O_2 does not increase as significantly. This effect has been shown to be beneficial in tissue engineered bone grafts[31,33] where the addition of a 10% PFTBA emulsion doubled bone volume after two weeks in one study[33]. While PFCs may help to reduce oxygen gradients within scaffolds, they do are unable to provide a reservoir or a prolonged release of oxygen sufficient to nurture cells within nascent tissue engineered grafts. Therefore, PFCs will likely only find a role as an adjunct to another oxygen delivery technology. The high cost of PFCs also limits their widespread adoption.

Peroxide-doped scaffolds rely on the decomposition of calcium peroxide[35], sodium percarbonate[40], among others[36], in the presence of water to generate oxygen for cellular consumption. This approach benefits from the relatively high density of oxygen contained within these materials and the ease of incorporating them into various polymeric scaffolds. Oxygen release has been demonstrated over periods of 4-10 days. The major concern with peroxide-doped scaffolds is the mechanism by which the oxygen is generated produces a number of intermediate reactive oxygen species and alkali byproducts. For example, calcium peroxide degrades[34] to produce hydrogen peroxide and calcium hydroxide, then hydroxyl and hydroxide, followed

by hydrogen peroxide anion, and then superoxide, before finally producing diatomic oxygen. Given that hydrogen peroxide can diffuse effectively 1.5mm within the extracellular fluid[41] there is concern that the reactive oxygen species could damage cells and negate the therapeutic benefit of the oxygen. For example, the reactive oxygen species generated from peroxides encapsulated within electrospun fibers have been shown to reduce bacterial growth[42]. Furthermore, the high amount of alkali byproduct (2 molecules per O_2) could affect pH.

Other technologies that have been investigated for oxygen delivery include hemoglobin-based oxygen carriers, ultrasonically driven oxygen generators, and lipid-stabilized oxygen emulsions. These approaches have demonstrated utility within other medical applications but are not suited for the requirements of tissue engineering. Thus there remains a significant need for approaches that can safely deliver oxygen within grafts over extended periods of time.

Biological and medical consequences of hyperoxia

With the discovery of the HIF pathway and its role in the production of VEGF to signal vessel ingrowth, it has become widely accepted within the tissue engineering community that moderate hypoxia is necessary for infiltration of surrounding vasculature into transplanted grafts. Thus there persists concern that oxygen delivery technologies will actually hinder vascularization. While there is certainly strong evidence to support the role of acute hypoxia in stimulating vascular infiltration, it is an error to assume the diametric condition of hyperoxia

must therefore inhibit vascularization. In fact, there have been a large number of studies that have demonstrated that hyperoxia can stimulate vascular assembly.

Hyperoxia is known to enhance wound healing in patients principally by stimulating angiogenesis and growth factor production[27–29], enhancing fibroblast proliferation, improving bactericidal function of leukocyte[25,26], increasing collagen deposition[43–45], reducing edema[46], and in cases of systemic hyperoxia mobilizing stem progenitor cells from the bone marrow[47]. With respect to VEGF production, a study monitoring the wound environment in rats receiving hyperoxic treatment found day 5 levels of VEGF elevated by 40% compared to controls, while lactate concentrations remained similar across groups. Maintaining levels of lactate is important because it signals the deposition of collagen by fibroblasts. The elevated levels of oxygen have been shown to increase the rate of collagen formation, specifically through the hydroxylation of proline and lysine. Additional studies have found elevated levels of fibroblast growth factor (FGF)[48], angiopoeitin 2 (Ang2), and platelet derived growth factor receptor (PDGF-R)[49]. Oxygen delivery does not suppress the formation of blood vessels[50].

CHAPTER II:

Theory of Oxygen Delivery Hyperbarically Loaded Materials

Diversity of Polymer Properties

Polymers are commonly utilized as structural components in tissue engineering scaffolds due to their suitable mechanical, biocompatible, and degradation properties in addition to being amenable to a number of bench-scale additive as well as subtractive manufacturing methodologies. Polymers offer incredibly diverse, and tunable physical properties over staggering ranges. However, it is important to consider that the vast majority of polymers being utilized in tissue engineering were specifically designed, at least initially, for other commercial applications and therefore can possess additional properties hereto unharnessed by tissue engineers.

Consider for example a bottle of Coca-Cola. The requirements for the bottle are: resilience against fracture, sufficient mechanical strength to contain pressure without deforming, and chemical/hydrolytic resistance to degradation – very similar requirements to scaffolds used in certain bone tissue engineering applications. In addition, the bottle needs to prevent CO_2 from escaping and leaving the soda flat. Thus it must possess an additional property known as a gas barrier property – the resistance of the material to permeation by a gaseous species. It is thanks to the incredibly diverse population of polymers that one exists to meet

these requirements, namely polyethylene terephthalate (PET), the stiff, transparent plastic now used ubiquitously in soft drink containers around the world.

Hitherto gas barrier properties have been largely the domain of packaging specialists and vacuum technologist with little regard given to them by tissue engineers who have almost by default treated the structural polymer portion of their grafts as impermeable and largely passive. However, just as in the example of the pop bottle, by looking to the origins of polymers and appreciating the breadth of their properties beyond the rudimentary mechanical properties, it is possible to engineer new and exciting functionality into what was once just structural scaffolding. It is from this perspective and motivation that we investigate the physics of gas transport within polymer systems with the aim of developing an oxygen delivery strategy for tissue engineering scaffolds.

Polymer Gas Barriers

We know from everyday experience that gases can permeate most solids. This is the reason a balloon will eventually deflate and why a pump is constantly needed to maintain a vacuum chamber. The degree to which gases permeate a solid depends on a number of factors (temperature, humidity, type of gas, pressure, and so forth) and can range over many orders of magnitudes, but the physical processes involved are common across materials, namely dissolution and diffusion.

The process of a gas entering a solid is known as dissolution and is governed by Henry's Law[51,52]:

$$c = sP^n$$

(II-1)

Where c is the concentration of gas within the solid, s is the solubility or amount of gas dissolved in the solid at STP, P is the pressure of the gas, and n depends on the material but is commonly 1 for non-metals. Thus it can be appreciated that the equilibrium amount of gas dissolved in a solid is proportional to the pressure of the gas in the environment around it.

At steady state, the movement of gas within the solid follows Fick's Law of diffusion[53]:

$$Q = D\frac{dc}{dx}$$

(II-2)

Where Q is the flux of gas, D is the diffusion coefficient of gas within the solid, and $\frac{dc}{dx}$ represents the concentration gradient of gas within the solid. The diffusion coefficient is considered independent of the concentration of gas in most applications.

Combining Fick's Law and Henry's Law, the permeation of gas through a membrane can be modeled as in Figure II-1. Consider that each side of the membrane has pressure P_1 and P_2, respectively. Then by Henry's Law we expect the concentration of gas at each side to be sP_1^n and sP_2^n, respectively. Now, assuming steady state, the concentration gradient across the membrane of thickness *d* will be:

$$\frac{sP_1^n - sP_2^n}{d}$$

(II-3)

Then by Fick's Law the flux is given by:

$$Q = D\frac{sP_1^n - sP_2^n}{d}.$$

(II-4)

This is the governing equation for permeation of gas through a barrier, but in practice for polymer systems, where n=1, the solubility and diffusion constants are typically grouped into a permeation constant σ resulting in the more tractable equation[54]:

$$Q = \frac{\sigma \Delta P}{d}$$

(II-5)

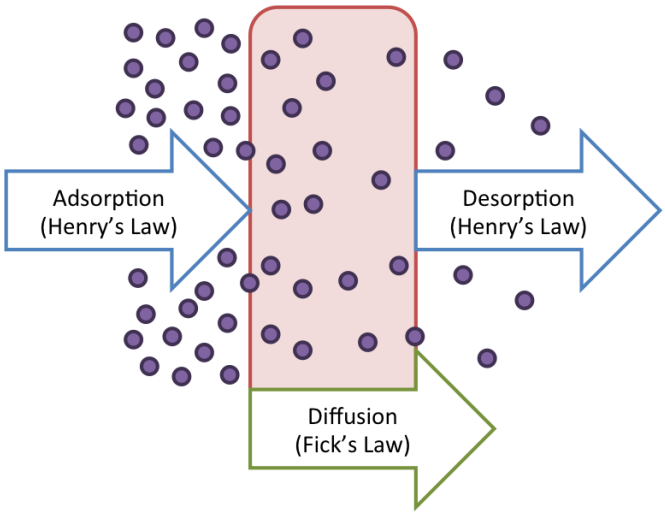

Figure II-1: Gas transport through a polymer slab involves adsorption, diffusion, and desorption. Gas dissolves into the polymer at the surfaces according to Henry's law. If a pressure differential is induced across the slab, then the concentration of dissolved gas particles will be higher on the high-pressure side. This concentration gradient will drive the diffusion of particles through the polymer to the low-pressure side where they will exit by desorption. Modified from Food Packaging Permeability Behaviour: A Report[55].

This equation is often sufficient for calculations involving the transport of gases into or out of packaging, as is commonly done for food or drug preservation. Of note from the equation are the limited variables that can be manipulated from a design perspective to modulate the flow of gas, specifically the thickness of the barrier and the barrier material of which σ is an intrinsic property, as the pressure difference is typically prescribed by the application (i.e. ambient to vacuum). From a practical perspective, the thickness of a barrier cannot be greatly varied, likely less than 3 orders of magnitude for most commercial applications. However, it turns out that the permeation constant σ varies tremendously across different polymers, up to 8 orders of magnitude. This provides the engineer with a means of making large steps in barrier properties by selecting different polymers and then fine tuning the properties by varying the thickness of the barrier. A list of commonly utilized polymers and their associated oxygen permeation properties is presented in Table 1 from Kuraray Corp[56] to give an idea of the magnitudes and range:

Table 1: Table of oxygen permeability values of commonly used packaging materials. (*P) indicated the permeability of the films in units of cm^3.20um/m^2.day.atm at a temperature of T in Kelvin (K=273+°C). Reproduced from Kuraray EVAL EVOH Resins Brochure[56]. The permeability of a polymer is a highly temperature dependent property, roughly doubling with a 10°C increase in temperature.

Films	Oxygen Transmission Rate at 0% RH (cm^3.20 µm/m^2.day.atm)				Permeability (*P) at 0% RH
	5°C	20°C	23°C	35°C	Formula
EVAL™ F type	0.06	0.2	0.25	0.6	$P = 1.42\ 10^{9}\ e^{-6647/T}$
EVAL™ E type	0.3	0.8	1.2	2.4	$P = 6.75\ 10^{8}\ e^{-5994/T}$
High barrier PVDC extrusion	0.74	2.6	3.2	8.1	$P = 3.31\ 10^{10}\ e^{-6822.5/T}$
$PVDC_{2\mu m}$ coated BOPP	2.2	10	13	32	$P = 2.36\ 10^{12}\ e^{-7693/T}$
PAN3	3	-	15.5	39	$P = 1.02\ 10^{12}\ e^{-7389/T}$
Oriented PA 6	9.7	28	33	64	$P = 2.77\ 10^{9}\ e^{-5408/T}$
Cast PA 6	28	-	100	194	$P = 1.37\ 10^{10}\ e^{-5560/T}$
Oriented PET	13	40	46	400	$P = 4.65\ 10^{15}\ e^{-9410/T}$
Rigid PVC	-	240	260	370	$P = 1.87\ 10^{6}\ e^{-2628/T}$
OPP	-	2,900	3,200	-	$P = 4.82\ 10^{7}\ e^{-2848/T}$
LDPE	-	10,000	10,900	-	$P = 4.95\ 10^{7}\ e^{-2493.9/T}$

Outgassing of a polymer slab

The fact that polymers can dissolve a significant amount of gas is not readily apparent from everyday experience, largely because the polymers are in equilibrium with the air and so the consequences are not readily observed. One tractable example however is the "new car" smell one detects in a recently manufactured automobile. This smell arises from gases and solvents trapped within the various polymers used to manufacture the car, seats, carpets, gradually diffusing out of the polymer and being released into the cabin air. This phenomena is called *outgassing* and occurs when a gas containing polymer is placed in an atmosphere without an equilibrium amount of gas. In most circumstances, outgassing is something to be avoided as it can increase the time required to pump down a vacuum chamber, introduce an unpleasant smell, or otherwise add a contaminant into a sensitive system. However, in the case of biomedical engineering the ability of polymers to dissolve and gradually release oxygen into the surrounding environment would be a major advantage. Thus we investigate the phenomena governing outgassing from a polymer slab.

The description of outgassing is really just the non-steady state (transient) description of the system used to develop the gas barrier equations and thus the two are intimately related. Consider an infinite polymer slab of thickness $2d$, centered at the origin, with a coefficient of diffusion D. Assuming the slab is in equilibrium with a gas, by Henry's Law we know that the initial concentration of gas within the polymer is $C_0 = sP$. If the slab is then placed in an environment so that the surface

concentration of gas is held at C_1, diffusion of the gas out of surfaces of the polymer will occur according to Fick's 2nd Law, resulting in a the concentration profile[57]:

$$\frac{C(t)-C_0}{C_1-C_0}=1-\frac{4}{\pi}\sum_{n=0}^{\infty}\frac{(-1)^n}{2n+1}exp\left\{\frac{-D(2n+1)^2\pi^2t}{4d^2}\right\}cos\left\{\frac{(2n+1)\pi x}{2d}\right\}$$

(II-6)

To calculate the amount of gas being delivered from a surface at any time, according to Fick's 1st Law of diffusion, one need only calculate the concentration gradient at the surface and multiply by the coefficient of diffusion:

$$ODR\ =D\left(-\frac{\partial C}{\partial x}\right)|_{x=\pm d}$$

(II-7)

Taking spatial derivative of the concentration profile and simplifying:

$$\frac{\frac{\partial C}{\partial x}}{C_1-C_0}=\frac{4}{\pi}\sum_{n=0}^{\infty}\frac{(-1)^n}{2n+1}exp\left\{\frac{-D(2n+1)^2\pi^2t}{4d^2}\right\}\left(\frac{(2n+1)\pi}{2d}\right)sin\left\{\frac{(2n+1)\pi x}{2d}\right\}$$

(II-8)

$$\frac{\frac{\partial C}{\partial x}}{C_1-C_0}=\frac{2}{d}\sum_{n=0}^{\infty}(-1)^n exp\left\{\frac{-D(2n+1)^2\pi^2t}{4d^2}\right\}sin\left\{\frac{(2n+1)\pi x}{2d}\right\}$$

(II-9)

Evaluating at the slab surfaces:

$$\frac{\frac{\partial C}{\partial x}|_{x=\pm l}}{C_1 - C_0} = -\frac{2}{d}\sum_{n=0}^{\infty} exp\left\{\frac{-D(2n+1)^2\pi^2 t}{4d^2}\right\}$$

(II-10)

Thus the outgassing from the face of each slab is described by the governing equation[53]:

$$ODR = \frac{2D(C_1 - C_0)}{d}\sum_{n=0}^{\infty} exp\left\{\frac{-D(2n+1)^2\pi^2 t}{4d^2}\right\}$$

(II-11)

The outgassing of a hyperbarically loaded polymer slab follows an exponential release with a time constant of:

$$\tau_{bulk\ phase} = \frac{4d^2}{\pi^2 D}$$

(II-12)

The initial phase of the release exhibits a sort of burst due to the contribution of the rapid exponential terms, but these quickly dissipate leaving a release profile dominated by the first exponential term. From the time constant, it can be observed that the period of outgassing is proportional to the square of the slab thickness and inversely proportional to the rate of diffusion. Thus, thicker slabs exhibit

considerably longer periods of outgassing compared to thinner slabs, and thickness becomes a means of tuning the period of outgassing.

Temperature Dependence of Permeation

The permeability of a polymer, σ, depends strongly on temperature. This is largely expected given that $\sigma = D \times S$ and both diffusion and solubility have temperature dependences, albeit exhibiting opposite trends.

For a gas to dissolve into a polymer two things must occur: 1) it must condense onto the polymer and 2) a molecular gaps large enough for the gas molecule must be created[58]. The partial molar enthalpy of sorption is thus represented by[58,59]:

$$\Delta H_S = \Delta H_{condense} + \Delta H_{mix}$$

(II-13)

For condensable gases the condensation term is dominant and negative, thus resulting in decreased solubility of gases at elevated temperatures[58]. This is highlighted in the van't Hoff equation[58,60]:

$$S(T) = S_0 \exp\left(-\frac{\Delta H_S}{RT}\right)$$

(II-14)

For diffusion, the opposite trend is observed with rates increasing with temperature. This is because the movement of gas molecules through the polymer

network is a thermally activated process[51]. The relationship can be expressed in the form of the Arrhenius equation with E_D the activation energy of diffusion[52]:

$$\mathrm{D(T)} = D_0 \exp\left(\frac{E_D}{RT}\right)$$

(II-15)

Compared to solubility, diffusion has a much greater temperature dependence and thus is the dominant term in the activation energy of permeation ($E_\sigma = E_D + \Delta H_S$), leading to the positive relationship between permeability and temperature[51]:

$$\sigma(\mathrm{T}) = \sigma_0 \exp\left(\frac{E_\sigma}{RT}\right)$$

(II-16)

This trend is generally true, although there can be exceptions around glass transition points.

The temperature dependence of permeability is important from a gas barrier perspective as relatively small changes in temperature can result in dramatic changes in permeability, as highlighted in Table 1. For polymers, the value of E_σ is commonly within the range of 1,000-10,000K [56], which means on average for a temperature increase of 10°C , around room temperature, one can expect the permeability of the polymer to roughly double. Conversely, for a temperature decrease of 10°C one would expect the permeability to decrease by half. Thus to increase or decrease the permeability by a factor of 1,000x it is only necessary to change the temperature by 100°C. This attribute can be harnessed for biomedical

applications and will be discussed in more detail later.

Outgassing of a hollow polymeric shell

Perfluorocarbon emulsions have been studied as a means of oxygenating blood and more recently as a means of delivering oxygen within a tissue engineered graft. While the capacity for perfluorocarbons to dissolve oxygen is impressive for a liquid (~50%V/V), their preparation as surfactant stabilized emulsions means that oxygen gas initially stored within the perfluorocarbon droplet rapidly diffuses out to equilibrate with the surrounding environment (useful for a circulating therapeutic that can be recharged each time it passes through the lungs, but useless as a reservoir for oxygen in a static application such as a tissue engineered scaffold). The ability to prolong the release of oxygen from perfluorocarbon droplets would allow significantly increase their utility within tissue engineering. To do so, would require the introduction of a gas barrier around the droplet to slow the release of gas and this motivates the study of gas delivery from a hollow polymeric shell.

Consider the geometry of the system: a sphere of radius r, with shell thickness d, which is composed of a polymer with gas permeability σ and is filled with gas at pressure P as in Figure II-2.

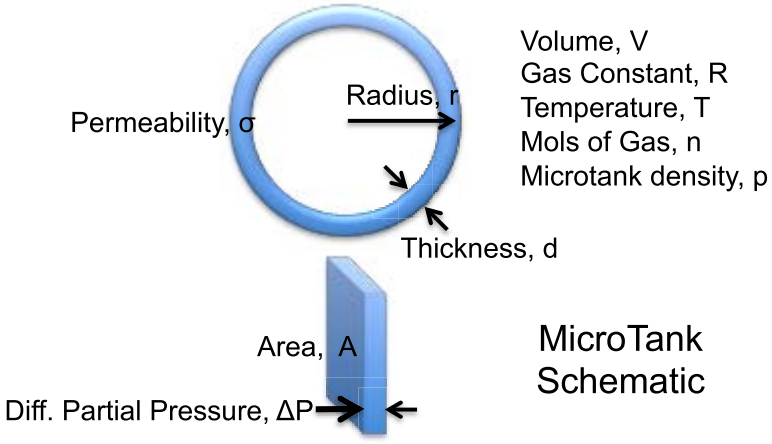

Figure II-2: Geometrical considerations of oxygen outgassing from a hollow polymeric shell or microtank. A microtank commonly has a spherical geometry with radius r, a shell thickness d, and is composed of a polymer with a permeability σ. Microtanks are commonly on the order of 100μm in diameter with a shell thickness of 1-10μm.

The amount of gas stored within the sphere initially is simply given by the ideal gas law:

$$PV = nRT \; or \; rearranged \; n = \frac{PV}{RT}$$

(II-17)

Taking the first derivative with respect to time, assuming the geometry and temperature of the system remain constant, demonstrates that the loss of gas from the hollow polymeric shell results in a proportional loss in pressure:

$$\dot{n} = \frac{V}{RT} \times \dot{P}$$

(II-18)

Within the system there is high pressure of gas within the core and a low pressure outside, separated by a relatively thin polymeric membrane. From the investigation of gas permeation earlier, it is established that gas will permeate through at a rate of:

$$\dot{n} = \frac{-\sigma \cdot \Delta P \cdot A}{d}$$

(II-19)

Due to the spherical geometry of the system, and the fact that the thickness of the polymeric membrane is thin with respect to the radius $\left(\frac{d}{r} \ll 1\right)$, the area available for permeation is:

$$A = 4\pi r^2$$

(II-20)

The equations for the change in gas $\dot{n}$ are interdependent through the pressure term. Thus by substituting one into the other, it is possible to understand the kinetics of the outgassing from the polymeric shell:

$$\frac{\dot{P}V}{RT} = \frac{-\sigma \cdot \Delta P \cdot A}{d}$$

(II-21)

The equations could be solved at this point, however, a simplifying assumption can be made with respect to pressure. It can be approximated that the driving pressure $\Delta P = P - P_{0_2 atm} \approx P$ because compared to the high pressure gas within

the core, the partial pressure of gas outside is approximately zero, especially in an *in vitro* or *in vivo* setting. This assumption does not affect the kinetics of the outgassing.

$$\dot{P} = \frac{-\sigma \cdot P \cdot A \cdot RT}{d \cdot V}$$

(II-22)

Substituting in for the known volume ($V = 4/3\pi r^3$) and area:

$$\dot{P} = \frac{-\sigma \cdot P \cdot 4\pi r^2 \cdot RT}{d \cdot 4/3\pi r^3}$$

(II-23)

Simplifying:

$$\dot{P} = \frac{-3 \cdot \sigma \cdot P \cdot RT}{d \cdot r}$$

(II-24)

And solving the ordinary differential equation:

$$\int \frac{dP}{P} = \int \frac{-3 \cdot \sigma \cdot RT}{d \cdot r} dt$$

(II-25)

$$\ln(P) = \frac{-3 \cdot \sigma \cdot RT}{d \cdot r} t + \ln(P_0)$$

(II-26)

$$\mathrm{P(t)} = P_0 \exp\left(\frac{-3 \cdot \sigma \cdot RT}{d \cdot r} t\right)$$

(II-27)

Results in the governing equation for outgassing from a hollow polymeric shell:

$$\mathrm{P(t)} = P_0 \exp\left(\frac{-t}{\tau}\right), where\ \tau = \frac{d \cdot r}{3 \cdot \sigma \cdot RT}$$

(II-28)

Thus theory predicts an exponential release profile, which intuitively makes sense because permeation of gas out of the core is proportional to pressure, which in turn is proportional to the amount of gas within the core. The time constant of release τ is also quite intuitive and informative. The time for release increases proportionally with the thickness of the shell and inversely with the permeability of the polymer. It also increases proportionally with the radius of the shell, which makes sense as smaller spheres have a higher ratio of surface area to volume and thus provide relatively more opportunity for permeation.

The rate of gas delivery or loss from the polymeric shell can be calculated by looking at the instantaneous change in the pressure equation:

$$\dot{\mathrm{P}}\mathrm{(t)} = \frac{P_0}{\tau} \exp\left(\frac{-t}{\tau}\right)$$

(II-29)

Or in terms of the molar delivery of gas:

$$\dot{n}(t) = \frac{VP_0}{RT\tau}\exp\left(\frac{-t}{\tau}\right) = \frac{n_0}{\tau}\exp\left(\frac{-t}{\tau}\right)$$

(II-30)

The above equations consider a single polymeric shell; however, if the outgassing from a collection of polymeric shells is desired then one must simply multiply by the volumetric density (polymeric shells / volume):

$$ODR = \rho \times \frac{n_0}{\tau}\exp\left(\frac{-t}{\tau}\right)$$

(II-31)

Substituting in all the parameters that can be tuned or selected produces the governing equation for the volumetric gas delivery from a dispersion of polymeric shells:

$$ODR = \frac{\rho(4\pi r^2 P_0)\sigma}{d}\exp\left(\frac{-t}{\frac{d\cdot r}{3\cdot\sigma\cdot RT}}\right), where\ \tau_{microtanks} = \frac{d\cdot r}{3\cdot\sigma\cdot RT}$$

(II-32)

For considerations of temperature, it is prudent to include the dramatic effects of temperature on the permeability of the polymeric shell, which exhibits an Arrhenius type behavior:

$$\tau = \frac{d \cdot r}{3 \cdot \sigma_0 \exp\left(\frac{-E_p}{RT}\right) \cdot RT}, where\ E_p\ is\ the\ activation\ energy\ of\ permeation$$

(II-33)

Mechanical Considerations

Prolonging the release of gas from a polymeric shell requires that the oxygen barrier remain intact and thus the mechanical strength of the vessel must be sufficient to contain the pressure. For a spherical geometry with radius r, cross sectional area A, circumference C, and tensile strength σ, the rupture pressure P can be easily calculated by considering the free body diagram of a central cross-section through the sphere as in Figure II-3.

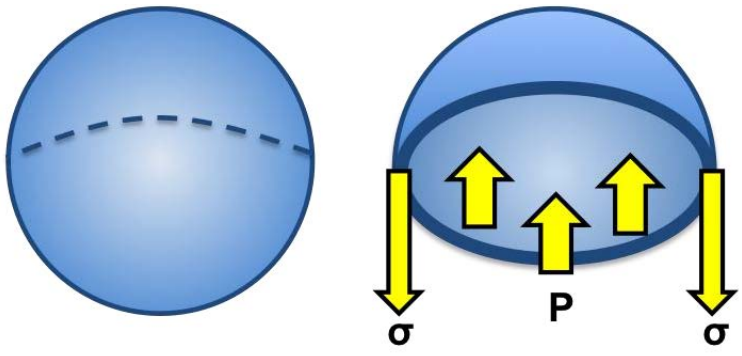

Figure II-3: Free body diagram of a spherical thin-walled pressure vessel. (Left) In the mechanical analysis, a central slice is made through the pressure vessel. (Right) The pressure P acting on the cross sectional area of the core generates a force P×A that must be balanced by tensile stresses σ in the shell.

For equilibrium, the force of pressure acting on the cross-sectional area must be balanced by tensile stresses in the wall. Thus:

$$PA = \sigma \mathrm{Cd}$$

(II-34)

$$P(\pi r^2) = \sigma(2\pi r)d$$

(II-35)

$$P_{rupture} = \frac{2\sigma \mathrm{d}}{r}$$

(II-36)

As an example calculation, reasonable values of tensile strength for polymers is 10-100MPa[61] and the polymeric shell typically has a radius of 50um and a thickness of 1um, so $P_{rupture} \approx 2\mathrm{MPa} \approx 20\mathrm{atm}$.

Analogously, for a polymeric closed-cell foam with an expansion ratio of 2:

$$P_{rupture} = \sigma \frac{\mathrm{A}_{polymer}}{A_{void}} = \sigma$$

(II-37)

One can expect a rupture pressure of 10-100MPa ≈ 100-1000atm.

Conception of Microtanks and Microtank-loaded Scaffolds

Upon considering the outgassing equations for polymeric slabs and thin-walled shells as well as the corresponding mechanical limitations, it is possible to

conceive of means to utilize these properties to deliver oxygen to cells within tissue engineered scaffolds (and numerous other applications as well).

The simplest conceptual implementation is to use microscopic polymeric shells with sufficient mechanical strength and oxygen barrier properties to store hyperbaric oxygen gas and gradually deliver this gas to the surrounding environment to nurture cells. By analogy to the scuba tanks used to maintain divers under water, such polymeric shells have been termed ***MicroTanks*** or ***microtanks***. Microtanks are capable of providing sustained oxygen delivery over an extended period of time. These hollow microspheres engineered from polymeric biomaterials can be hyperbarically loaded with oxygen. The intrinsic permeability of the polymer, which forms the surrounding shell, regulates the outward diffusion of oxygen along the pressure differential into the surrounding environment. By varying the composition of the polymer, the thickness of the shell, the diameter, or the pressures to which the microtanks are loaded, it is possible to finely tune the rate and duration of oxygen delivery to the surroundings from several hours up to two weeks.

Within the subset of scaffolds designed for orthopedic applications, there is a commonly a structural phase made out of a relatively stiff, robust polymer and a hydrogel phase made up of growth factors, ECM proteins, and nutrients. By forming the structural phases out of a polymer with sufficiently low oxygen permeability and incorporating in microtanks, it would be possible to add oxygen functionality to an otherwise inert component. Experimental validation of this approach follows in Chapter III.

Outgassing from Composites of Microtanks Suspended in Bulk Polymer

In the case where a syntactic foam has been created by combining microtanks within a bulk polymer phase, the outgassing kinetics vary according to the relative contributions of the outgassing phenomena. One must consider that in such a system, oxygen must permeate 1) from the core of the microtank through the shell into the bulk polymer and 2) through the bulk polymer out to the scaffold-hydrogel interface. In the case where the outgassing from the microtanks is very slow compared to outgassing from the bulk phase (e.g. very thin slabs), the kinetics are determined by the microtanks. Conversely, if the outgassing from the slab is very slow compared to the microtanks, then the kinetics are governed by the slab. If the kinetics of outgassing are comparable between the two stages, then the overall kinetics are approximately the sum of the individual kinetics. Generally speaking, outgassing of a composite scaffold occurs as:

$$\tau_{outgass} = \tau_{microtank} + \tau_{bulk\ phase}$$

(II-38)

CHAPTER III:

Oxygen Delivery from Hyperbarically Loaded MicroTanks Extends Cell Viability in Hypoxic Environments

Manuscript for Publication

The following chapter is written as a manuscript for submission to an academic journal. It covers the empirical data collected to validate the outgassing theory described in Chapter II as well as *in vitro* data to validate the therapeutic effect of oxygen delivery in hypoxic environments.

Hyperbaric Chamber Apparatus

The hyperbaric chamber referred to within the manuscript was designed using thick-walled pressure vessel analysis, confirmed by FEM modeling in COMSOL, and manufactured in the BME Machine Shop by Jay Burns. The chamber is rated for operation up to 100atm and has been designed for use with pure oxygen. It includes a quick-connect fitting for connection to the high pressure oxygen tank, a bleed valve to return the chamber to atmospheric pressure, a pressure relief valve to vent gas in the case of over-pressurization, and a pressure gauge to monitor chamber pressure. The feed line from the high-pressure oxygen regulator is terminated with a one-way/check valve to prevent blowback into the main tank. The chamber is seen here in Figure III-1.

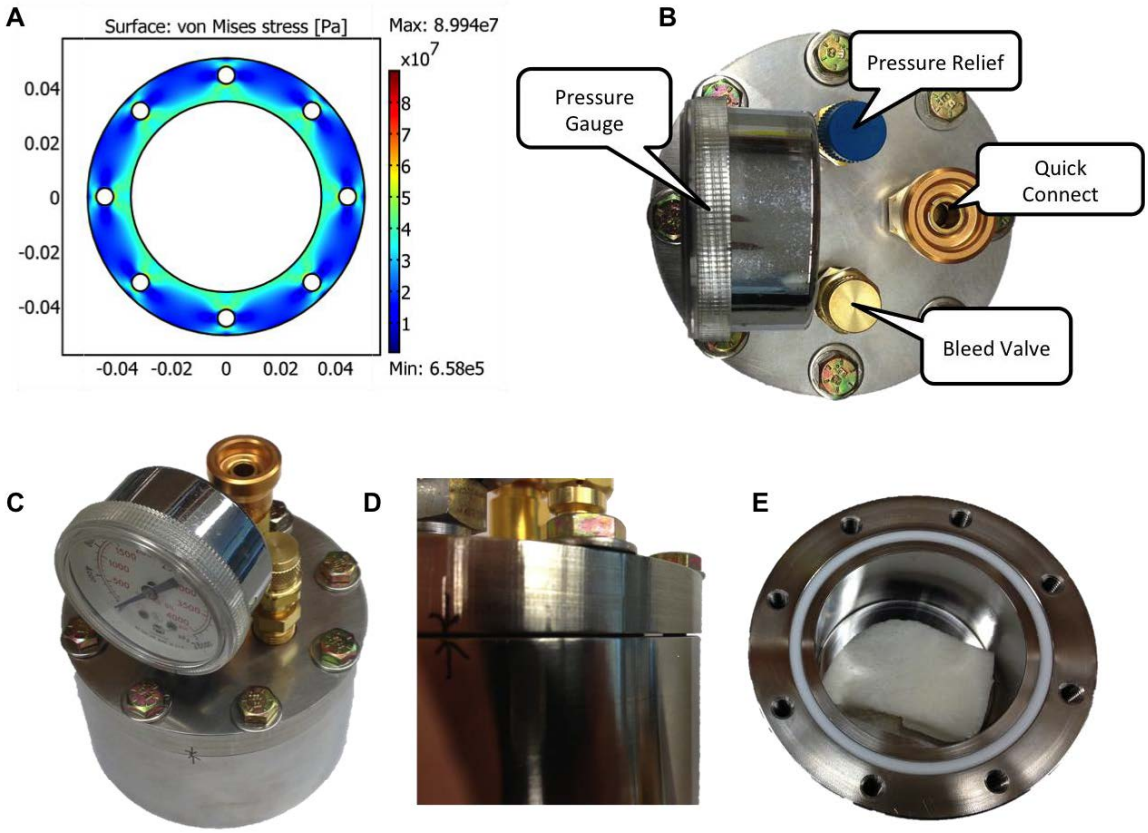

Figure III-1: A hyperbaric chamber is used to load scaffolds and microtanks with oxygen. (A) COMSOL FEM modeling was used to ensure a factor of safety of 3 while operating within the design limit of 100atm. (B) Valve layout of hyperbaric chamber: bleed valve allows depressurization, pressure gauge provides pressure readout, pressure relief valve provides protection against over-pressurization, and quick connect valve allows for easy attachment to the high pressure regulator and oxygen tank. (C) View of assembled hyperbaric chamber. (D) Side view of lid, Teflon O-ring gap, and base, with high tensile strength bolts. (E) 2.5-inch diameter by 2-inch deep chamber fits a pig mandibular scaffold.

INTRODUCTION

Tissue engineered bone, muscle, liver, fat, and blood vessels have all been successfully demonstrated in small animal models. These successes are a bellwether of the promise of regenerative medicine to revolutionize healthcare by providing patient-specific grafts to replace damaged or failing tissue. These reports have helped establish the underlying biology of tissue formation and provided an encouraging proof-of-concept; however, they often overlook the challenges[1–4] associated with scaling the grafts from the mm^3 domain of mice and rats to the cm^3 domain of humans.

Within small grafts the process of diffusion alone can accommodate the transport of nutrients, oxygen, and waste, where as in larger, so-called diffusion-limited grafts, convection is required to meet metabolic needs. Unfortunately, convection requires functional vascular networks[5,6] and these can take several days to weeks to form. During this period, cellular metabolic demand exceeds supply leading to nutrient deficiency and hypoxia[1,7,8], which can lead to cell death and graft failure if persistent.

Diffusion limitations apply to all metabolic molecules and can be estimated by comparing rates of delivery and/or generation to rates of consumption, as is captured in the Thiele modulus[9] (1D case): $\phi = h\sqrt{\frac{\rho_{cell} V_{max}}{K_m D}}$, with scaffold thickness h, cell density ρ_{cell}, cellular oxygen uptake rate V_{max}, Michaelis constant K_m, and oxygen diffusion D. A large Thiele modulus indicates diffusion limitations and hence the presence of gradients. When considering cell metabolism both the deficit of

nutrients as well as the accumulation of waste products can be problematic[10,11]. However, in examining the prototypic equation of glucose metabolism it becomes apparent that oxygen is of special importance[3,6]. If oxygen is present, cellular respiration is able produce 30 ATP per glucose molecule and the relatively fast diffusing CO_2 waste product where as if oxygen is not available anaerobic glycolysis is only able to net 2 ATP plus the relatively slow diffusing lactic acid waste product[7,12]. The fact that oxygen directly impacts the diffusion limitations of glucose and waste products underscores the two-fold dangers of hypoxia within tissue-engineered grafts.

Given the deleterious consequences of hypoxia within diffusion-limited grafts, a number of approaches have been investigated to augment oxygen supply within nascent grafts to maintain cell viability during the period of vascularization. These have included: hyperbaric oxygen therapy where the patient and/or graft is placed in an oxygen enriched environment to enhance the oxygen content dissolved in the blood and interstitial fluid[24,27–29], perfluorocarbon emulsions which utilize the high oxygen solubility properties of these chemicals to enhance diffusion rates[2,30–33], and various peroxide compounds which generate oxygen during a decomposition reaction[34–36]. While each of these approaches has highlighted the benefits of oxygen augmentation, they unfortunately each suffer from limitations in terms safety and/or efficacy that have prevented their widespread adoption. Thus there remains a significant need for approaches that can deliver oxygen within grafts over extended periods of time.

In this paper, we describe a novel oxygen delivery strategy, which avoids many of the drawbacks of previous approaches. The approach centers around a microscopic hollow polymeric balloon that can be hyperbarically loaded with oxygen and subsequently release the gas back into the surrounding environment to nurture cells over an extended period of time. As the cellular analogue to a scuba tank we have termed these oxygen carriers: *MicroTanks* and they are diagramed in Figure III-2. The polymeric shell of the microtank provides dual functions: mechanical confinement of the pressurized oxygen and a gas barrier to control the diffusion of oxygen out of the hollow core. With interest in bone tissue engineering, the microtanks were combined into the structural polycaprolactone phase of scaffolds. Thus in our system oxygen diffuses out of the microtanks, through the bulk PCL phase, and ultimately into the hydrogel phase where it is consumed by cells. The aim of this paper is to lay the theoretical framework for the microtank approach and provide experimental evidence to demonstrate consistency and efficacy.

MATERIALS & METHODS

Fabrication of Microtank Containing Scaffolds

Scaffolds containing microtanks were fabricated by melting polycaprolactone (InstaMorph, USA) at 100°C and combining with commercially available microballoons E030 (Henkel, CT, USA). The mixture was then cast into sheets of varying thicknesses and subsequently formed into disks using a hand punch (14mm diameter).

The final concentration of microtanks by volume was calculated by casting a 200um sheet of the mixture, imaging using a bright field microscope, and using ImageJ to quantify the volume of microtanks within the known volume of the imaged material.

Loading of Microtank Containing Disks

Disks and scaffolds were loaded with oxygen in a custom built hyperbaric chamber. The chamber was loaded to pressures of 10-20atm with pure oxygen for a periods equal to at least 3 times the periods of release for the disks. In some instance, disks were removed from the chamber following loading to prerelease for a given period before starting an experiment to provide different levels of oxygen delivery.

Quantitative Measurement of Oxygen Release Profiles

A Seahorse XF^{e}24 Extracellular Flux Analyzer (Seahorse Bioscience, USA) was used in conjunction with islet plates to provide quantitative measurement of

oxygen release from the scaffold material. Briefly, the polycarbonate XF24 Islet Capture rings were filled with the scaffolds material, hyperbarically loaded with oxygen, and then placed within the 24-well microplate. The disks were covered with 625uL of XF solution and the delivered oxygen was allowed to diffuse to atmosphere. Individual oxygen probes monitored the oxygen levels within the solution at increments of 20minutes for the first 6 hours and every 30minutes thereafter. Changes in oxygen levels over time were used to produce an oxygen delivery plot.

Visualization and Semi-quantitative Measurement of Oxygen Release

A colorimetric assay for oxygen release from scaffolds was developed to provide visual corroboration to oxygen probe-based methods. A solution of oxygen sensitive resazurin dye (3mL of 0.1%), sodium hydroxide (1M), and glucose (0.133M) was prepared that turns pink in the presence of oxygen and clear in the absence of oxygen. This occurs by the oxidation of the dye through the conversion of glucose to gluconic acid. As the oxygen is consumed in the reaction, this solution enables the observation of quasi-steady state oxygen delivery rates from scaffolds, where the intensity and thickness of the pink band emanating from the scaffold surface is proportional to the flux of oxygen.

To measure the flux of oxygen, 14mm diameter disks of various thicknesses composed of PCL and microtanks were cast, loaded with oxygen, and mounted vertically to a weighted support structure so their profile could be observed. The disks were placed in a glass enclosure, submerged in fresh resazurin solution, and

allowed to reach quasi-steady state (~5min). A digital camera was used to take images of the disk profile and resazurin bands.

The widths of the bands are quantified using a custom Matlab program. Briefly, the program aligns the disk to 90 degrees, crops the central 1/3 of the disk, extracts the green channel for maximum contrast, plots the average intensity (gray value) of the image from which the widths of the resazurin band and the disk are extracted. In the green channel the resazurin band shows up as a dark region in contrast to the white disk and background, producing a valley shape in the profile plot. For consistency, the width of the band is taken as the width at half-maximum of this valley. For each image, the pixel width of the bands from left and right faces are measured, averaged, and normalized by the pixel width of the disk to compensate for any variations in zoom of the image.

Cell Culture and Media Conditions

Timecourse

Human ASCs (Passage 3-5) were combined into fibrin gels (8mg/mL bovine fibrinogen, 2U/mL thrombin, in PBS) and cast into 100uL gels in a polycarbonate 4mm inner diameter mold at a cellular concentration of 2,500 cells/uL. The polycarbonate disks were positioned on top of the PCL and microtank disk samples (12mm diameter x 4mm thick), which were glued to the bottom of 12-well plates. Three groups of identical microtank filled PCL disks were used (n=4): Neg, in which the disks were purged with nitrogen, Pos, in which the disks were equilibrated in

atmosphere, and uTank, in which the disks were loaded in 100% O_2 at 15atm and allowed to pre-release for 24hrs before cell seeding.

Cells were fed with 2mL of expansion medium (89mL Low Glucose DMEM, 1mL FBS, 1mL P/S, 20uL FGF) and then placed in anoxic chambers, which were purged for 15min with anoxic gas mixture (5% CO_2 + 95% N_2) then sealed closed. The chambers contained oxygen-absorbing packs to quench any released oxygen. Chambers were incubated at 37°C and contained a water reservoir to maintain humidity. Pos were cultured under normoxia (21% O_2 + 5% CO_2 + 74% N_2). Samples were removed at Day 0, Day 2, Day 4, Day 6, and Day 8 time points for analysis.

Oxygen Sensitivity

Human ASCs and HUVECs were combined (ratio of 2.5:1) at 2,500 cells/uL into fibrin gels and cultured on disks similarly to the timecourse study with the following groups (n=4): Neg, in which the disks were purged with nitrogen, Pos, in which the disks were equilibrated in atmosphere, and uTank (High, Med, Low), in which the disks were loaded in 100% O_2 at 15atm and allowed to pre-release for 30, 54, and 78hrs, respectively, before cell seeding. Cells were fed with 2mL of expansion medium (89mL Low Glucose DMEM, 1mL FBS, 1mL P/S, 20uL FGF) and then placed in anoxic chambers, which were purged for 15min with anoxic gas mixture (5% CO_2 + 95% N_2) then sealed closed. The chambers contained oxygen-absorbing packs to quench any released oxygen. Chambers were incubated at 37°C and contained a water reservoir to maintain humidity. Samples were removed at Day 6 for analysis.

Vascular Assembly

Human ASCs and HUVECs were combined at 2,500 cells/uL each into fibrin gels and cultured on disks similarly to the timecourse study with the following groups (n=4): Neg, in which the disks were purged with nitrogen, Pos, in which the disks were equilibrated in atmosphere, and MicroTank, in which the disks were loaded in 100% O_2 at 15atm and allowed to pre-release for 30hrs before cell seeding. Cells were fed with 5mL of endothelial cell media and then placed in anoxic chambers, which were purged for 15min with anoxic gas mixture (5% CO_2 + 95% N_2) then sealed closed. The chambers contained oxygen-absorbing packs to quench any released oxygen. Chambers were incubated at 37°C and contained a water reservoir to maintain humidity. Samples were removed at Day 4 for L/D analysis.

PicoGreen DNA Assay

The PicoGreen assay was carried out according to the manufacturer's instructions. Gels were transferred into 600uL of TEX + Proteinase K and frozen at -20°C. Samples were subsequently heated at 55°C overnight to digest proteins and lyse cells. The samples were combined with PicoGreen reagent (20uL sample + 80uL TEX + 100uL PicoGreen) and transferred (200uL) into opaque 96-well plate along with DNA standards. Fluorescence was measured at 485/528 using a plate reader.

Alamar Blue Assay

A solution of 0.001% resazurin in expansion media was prepared fresh and added at 2mL/well to a 24-well plate. Gels were transferred individually into the

wells and allowed to incubate for 2hrs at 37°C in the incubator. 200uL samples of the solution were placed in opaque 96-well plates and measured using fluorescence spectrometry at 540/590nm using a plate reader.

Predictions of Cellular Oxygen Uptake Rates

Cellular uptake rates for human endothelial and adipose derived stem cells were obtained from the literature[62,63]. The metabolic demand of cells was estimated as the product of cell density, specific cellular oxygen uptake rate, and gel volume.

RESULTS

Governing Equations of Oxygen Delivery from Microtank Containing Scaffolds

Upon hyperbaric loading, oxygen enters the microtanks according to the ideal gas law $C = \frac{\Phi P}{RT}$ and dissolves in the bulk PCL according to Henry's law $C = S(1 - \Phi)P$, where Φ is the volume fraction of microtanks, P is the loading pressure, R is the ideal gas constant, T is temperature, and S is the solubility constant of oxygen in polymer. Thus at equilibrium the concentration of oxygen is proportional to the loading pressure and the volume fraction of microtanks as:

$$C = \left[\frac{\Phi}{RT} + S(1 - \Phi)\right] P.$$

In order for gas to be delivered from the scaffolds it must diffuse from the microtanks through the PCL to the scaffold surface. While the kinetics of the delivery will vary according to geometry, for the simple case of outgassing from a slab the delivery of gas from the surface goes as:

$$ODR = \frac{2c_1 D}{d} \sum_{i=1}^{i=\infty} \exp\left(\frac{-(2i-1)\pi^2 Dt}{4d^2}\right), where\ \tau_{bulk\ phase} = \frac{4d^2}{\pi^2 D}.$$

In addition to the diffusion of gas through the bulk polymer phase, oxygen must also permeate through the thin polymeric shell of the microtanks. The rate of transport ($\dot{n}$) of a gas through a thin membrane is proportional to the pressure drop (ΔP) across the membrane, the area (A) of the membrane, and the permeability (σ) of the membrane to the gas, which is the product of the solubility diffusion of the gas

within the polymer ($\sigma = D \times S$), while inversely proportional to the thickness (d) of the membrane: $\dot{n} = \frac{-\sigma \cdot \Delta P \cdot A}{d}$. Thus for a microtank of radius (r) loaded to a pressure (P_0) the oxygen delivery rate follows the exponential form:

$$ODR = \frac{\rho(4\pi r^2 P_0)\sigma}{d} \exp\left(\frac{-t}{\frac{d \cdot r}{3 \cdot \sigma \cdot RT}}\right), where\ \tau_{microtanks} = \frac{d \cdot r}{3 \cdot \sigma \cdot RT}$$

Thus the oxygen delivery from hyperbarically loaded microtank containing scaffolds exhibits an exponential delivery profile combined of components from the bulk phase and the microtank phase. As an approximation the time constant of oxygen delivery is the sum of the time constants of the constitutive phenomena: $\tau_{outgass} = \tau_{microtank} + \tau_{bulk\ phase}$.

To validate the theory governing oxygen delivery from microtank containing scaffolds, PCL disks with and without microtanks were fabricated, loaded with oxygen, and then the oxygen delivery rate was monitored using a Seahorse XF^{e}24 Extracellular Flux Analyzer. The profiles, illustrated in Figure III-3**a**, were fitted with the theoretical equation to extract time constants and integrated to calculate the total oxygen content within the disks, summarized in Figure III-3**b**. The microtank loaded disk is observed to have a significantly higher time constant than the disk without, suggesting the microtanks contribute significantly to slowing the release of gas from the disks. Additionally, the total oxygen content in the microtank-loaded disks is roughly 3x that of the disk alone, demonstrating the ability of microtanks to significantly increase the capacity of hyperbarically loaded materials.

Colorimetric Assay of Oxygen Delivery

In scaling to larger scaffolds, the Seahorse XF^{e}24 Extracellular Flux Analyzer is no longer suitable for monitoring oxygen release so we developed a semiquantitive colorimetric assay to allow for visual monitoring of oxygen delivery as well as extraction of time constants of release. The assay utilizes the color changing properties of resazurin dye in the presence of oxygen to spatially indicate oxygen delivery. By imaging scaffolds successively over time and monitoring the intensity and widths of the resazurin bands emanating from the scaffolds it is possible to further characterize the oxygen delivery temporally. Figure III-4 highlights this method. Again, the release profile is consistent with the theory.

Tuning Oxygen Delivery Profiles

We sought to further characterize the oxygen delivery in larger scaffolds as a function of scaffolds thickness. As shown in Figure III-5, disks with thicknesses of 1mm, 2mm, and 4mm were fabricated, loaded with oxygen, and then monitored by the resazurin assay for the kinetics of oxygen delivery. The release profile obtained was fitted with the theoretical release profile to extract a time constant of release. It is observed that thicker disks exhibit significantly longer periods of release. This trend is consistent with the theory; however, the relationship is expected to be 2nd order where as empirically it is observed to be between 1st and 2nd order.

Additionally, the relationship between microtank concentration and oxygen delivery was investigated. Briefly, PCL disks containing 0%, 1.4%, or 7% V/V microtanks were fabricated, loaded with oxygen, and monitored by resazurin assay for oxygen release. The relative flux of oxygen from the disks was compared as is summarized in Figure III-6, suggesting that oxygen delivery can be tuned by increasing the concentration of microtanks within the scaffold.

Scaffold Storage

From the theory, it is observed that the time constant of oxygen delivery is inversely proportional to the rate of diffusion within the polymer. It is well established that diffusion is a temperature dependent property; however, as temperature increases the solubility of gases within the polymer decreases. The net effect of these competing phenomena is best captured in the gas permeability ($\sigma = D \times S$), which has the form $\sigma(T) = \sigma_0 \exp\left(\frac{-E_P}{RT}\right)$. For polymers E_P/R is commonly on the order of 5×10^3 K (EVOH manual), so around room temperature a decrease of 10°C will halve the permeability. We therefore sought to investigate if cooling could provide a facile means of storing and shipping loaded scaffolds prior to implantation.

Disks of PCL containing microtanks were loaded with oxygen and then stored for 1 week at ambient pressure at 20°C, -20°C, or -80°C, or at loading pressure in the hyperbaric chamber. Following the week of storage, the magnitude of oxygen delivery from the disks was compared using the resazurin assay. The results of this experiment are summarized in Figure III-7 and reveal that disks stored at -20°C and

-80°C have maintained equivalent oxygen content to freshly loaded disks (i.e. those stored within the hyperbaric chamber). In contrast, disks stored at 20°C has significantly less oxygen content than all groups. While not statistically significant, the disks stored at -80°C maintained slightly higher oxygen content than those at -20°C.

Time course of Therapeutic Effect

Having characterized the delivery of oxygen from microtank containing disks, the therapeutic potential to extend cell viability in hypoxic environments was assessed by monitoring cellular metabolism over time with and without microtank-loaded scaffolds. Briefly, an Alamar Blue assay was used to measure the metabolism of ASCs cultured on PCL disks in 100uL 3D fibrin gels under anoxic conditions out to 8 days. The 4mm disks from the characterization experiments were used, as they possessed the largest time constant. Anoxic culture conditions (0% O_2, 5% CO_2, 95% N_2) were used to simulate the worst-case scenario within diffusion limited grafts. Positive controls groups were cultured under "normoxic" conditions (21% O_2, 5% CO_2, 74% N_2) to provide a benchmark.

At each time point, the relative metabolism of the cells normalized to the positive control was measured and the results are presented in Figure III-8. It can be observed that the metabolism of the negative control group, which contained scaffolds without microtanks, drops steadily under anoxia. In contrast, the group containing microtanks maintains appreciable metabolism out to Day 4 before

beginning to drop off at Day 6. This suggests that the oxygen delivery from the microtank loaded scaffolds is able to provide a therapeutic benefit to ASCs under anoxic conditions.

Sensitivity to Oxygen Delivery vs Cellular Demand

Having demonstrated that cell metabolism under anoxic conditions can be extended using microtank loaded scaffolds, we sought to investigate how the amount of oxygen delivery affected cell growth. Three different amounts of oxygen delivery were selected, based upon predicted cellular demand, to be higher, lower, or equal to demand. Figure III-9**a** illustrates the ratio of $\frac{oxygen\ demand}{oxygen\ delivery}$ over time based on the measured oxygen uptake rate for ASCs from the literature and the previously measured oxygen delivery rate for the disks over time.

Cell growth was determined by measuring DNA content at Day 6, the previously determined therapeutic limit for these scaffolds, by PicroGreen Assay. A similar experimental setup was utilized. The results of this experiment are summarized in Figure III-9**b** and several notable trends are observed. Firstly, all microtank containing scaffolds performed significantly better than the negative control. Secondly, the cell growth in the microtank groups correlates with the amount of oxygen delivered, with groups receiving more oxygen exhibiting more growth. Thirdly, cell growth in the microtank groups is comparable to the positive control.

Oxygen Delivery Enhances Vessel Formation

Co-cultures of ASC:HUVECs demonstrated expansion and elongation after 4 days in fibrin gels. Live/dead confocal imaging of the gels, Figure III-10**A**, demonstrates a higher proportion of live cells within the Positive and MicroTank groups compared to the Negative group. Quantification of the ratio of live/dead cells, Figure III-10**B**, is similar between the Positive and Microtank groups, where as the Negative group displays significantly less viable cells than the MicroTank group, highlighting the therapeutic benefit of oxygen delivery.

DISCUSSION

The use of oxygen outgassing from hyperbarically loaded scaffolds to maintain cell viability under hypoxic conditions, in so far as we are aware, represents a completely novel therapeutic approach. The approach provides a number of advantages when compared to previously described oxygen delivery technologies. Firstly, there are no cytotoxic byproducts produced in contrast to peroxide-based approaches, which release reactive oxygen species intermediates, acid, and commonly Ca^{2+} stoichiometrically with each O_2 molecule generated. Secondly, the system has a relatively high oxygen delivery capacity as compared to perfluorocarbon-doped scaffolds, which are only able to contain approximately 50% v/v O_2 at 1 atm, allowing for sufficient oxygen for nearly a week and possibly longer. Thirdly, the approach is highly tunable and the oxygen delivery characteristics have been well established.

The aim of this paper was to present the governing principles, proof-of-concept, and therapeutic benefit of the microtank approach. Therefore, there are a number of elements that need addressing before it could be considered as clinically viable, but we do not believe they undermine the long-term feasibility of the approach. Firstly, the use of polyacrylonitrile microballoons within the system is not appropriate for translation due to long-term biocompatibility concerns and toxic degradation products. However, these could be substituted for microballoons made of a more suitable polymer, such as a PLGA, and in fact we have begun working on developing biocompatible/bidegradeable microtanks with this in mind. Secondly, the use of PCL may not be appropriate for all applications; however, given its ease-

of-use and low melting point it allowed for the bench-top fabrication of scaffolds, obviating the need for expensive processing equipment necessary for other thermoplastics. Finally, the geometries and scaffold sizes used within this study have not been selected for a specific application, but could be formed into appropriate shapes using 3D printing, injection molding, thermoforming, etc. The scaffold thicknesses utilized were necessary to achieve biologically meaningful periods of oxygen release; means of addressing this limitation are subsequently discussed.

The loading and storage of microtank containing scaffolds presents a couple of logistical challenges. Firstly, with loading the time to equilibrium is approximately 4-5 time constants; however, for scaffolds with periods of release of even 48 hours this can become time consuming. It is unlikely that such turn around times would be accepted in a medical setting. Fortunately, by loading the scaffolds at elevated temperatures, well below melting point, it should be possible to greatly reduce loading times by 1 to 4 orders of magnitude, i.e. down to hours and minutes. This will require a hyperbaric chamber designed for operation at elevated temperatures and safety considerations given the use of pressurized oxygen but is well within the realm of technical feasibility. The second challenge relates to the storage of oxygen-loaded scaffolds. However, as we have demonstrated the cooling of scaffolds significantly enhances the shelf life and by theoretical estimates storage to outwards of 35 to 15,000 times the period of release are expected for -20°C and -80°C, respectively. These findings improve the translational potential of the microtank approach.

While this work has primarily relied on the bulk PCL polymer phase of the scaffolds to control and extend the release of oxygen, it may be possible to engineer the microtanks themselves to provide the necessary oxygen barriers. In the current system, the time constant of release is directly related to the scaffold geometry. This places constraints on the possible geometries that can be formed while maintaining therapeutically meaningful periods of oxygen delivery. In contrast, if the microtanks themselves had the desired period of release then there would no longer be practical limitations on geometry beyond the dimensions of the microtanks. This would require the thin polymeric shell of the microtank to have a high oxygen barrier, such as that afforded by polyvinyl alcohol (PVA). The development of PVA microtanks is thus an ongoing aim of our laboratory.

Alternatively, it may be possible to utilize a bulk phase polymer with significantly lower diffusion rates of oxygen than PCL to increase the period of oxygen delivery out to 2-3 weeks without the need to utilize impractically thick segments of scaffolding. Dacron (a.k.a. polyethylene terephthalate) has approximately $1/10^{th}$ the diffusion constant as PCL and therefore may be a suitable replacement. By utilizing a constant diameter filament/strut size, uniform oxygen delivery throughout a complex shaped scaffold could be accomplished through 3D printing methods. The results from this study compel us to work to extend the release profile of hyperbaric loaded microtank containing scaffolds to overcome the acknowledged limitations of PCL scaffolds, thus enhancing the overall therapeutic impact.

An important finding of this study was that oxygen delivery could support vessel formation under anoxic conditions. This suggests that it may be possible to maintain cells in vivo long enough for functional vasculature to develop to nurture the graft. While these results provide proof of concept, additional studies will be required to evaluate the robustness of the vessel formation, optimize the cell seeding density and oxygen delivery, and characterize the kinetics of vessel formation.

CONCLUSION

The outgassing of hyperbarically loaded materials has the potential to mitigate the negative effects of hypoxia within tissue-engineered grafts, especially where the graft contains a structural phase in addition to a hydrogel phase. The approach can add oxygen delivery functionality in a facile and predictable manner. The local delivery of oxygen may produce similar therapeutic benefits to hyperbaric oxygen therapy, without the need for systemic delivery and expensive and cumbersome chambers. Beyond tissue engineering the approach may hold promise to reduce infections, increase collagen deposition, and enhance healing, which would make it particularly attractive for use in medical fasteners such as screws, plates, and sutures. The diverse applications and implementations of the approach together with its simplicity make it an exciting platform for future studies.

FIGURES

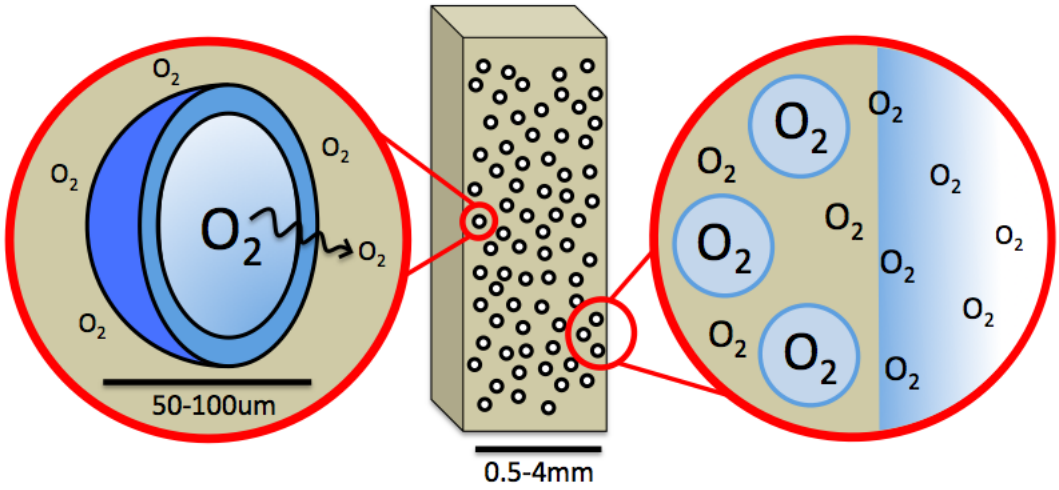

Figure III-2: Schematic of microtank loaded PCL scaffolds. Scaffolding material composed of PCL is embedded with microtanks to create a syntactic foam with distributed closed-cells. The microtanks contain a hollow core, which can be hyperbarically loaded with gaseous oxygen, surrounded by a polymeric shell composed of a structural, oxygen barrier layer to contain the pressurized oxygen. The pressure differential across the microtank shell drives the outward diffusion of oxygen through the shell and into the bulk PCL where it continues to diffuse out to the periphery of the scaffolding and into the media/hydrogel to nourish cells. The release of oxygen from microtank embedded scaffolds is regulated by the rate of permeation through the shell plus the rate of permeation through the bulk phase.

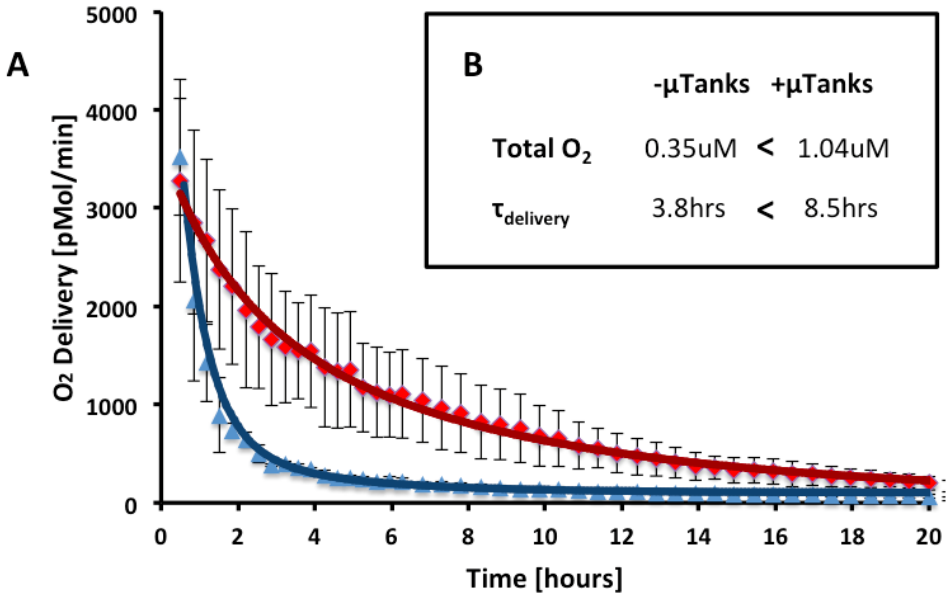

Figure III-3: Microtanks enhance oxygen delivery capacity and duration. (A) Oxygen delivery from hyperbarically loaded disks with microtanks (+uTanks) compared to without (-uTanks), fitted with theoretical delivery profile to extract time constants of delivery. (B) Total oxygen delivered was calculated by integrating the delivery curves while time constants of delivery were calculated from fit.

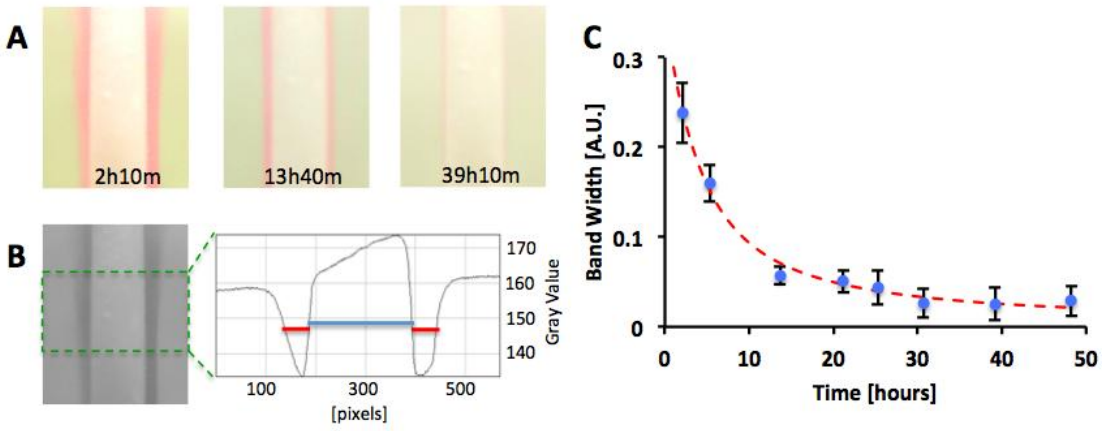

Figure III-4: Resazurin assay provides colorimetric visualization and quantitation of oxygen delivery duration from microtank containing PCL disks. (A) Photograph of 2mm thick disks in resazurin solution indicating oxygen release (pink) over a period of 2 days. (B) Green channel of photographs (left) are used to quantify the thickness of the resazurin bands emanating from the disks by plotting the average horizontal profile of the image (green box) and extracting the band widths (red) and disk thickness (blue) at half maximum. (C) Plotting the thickness of the resazurin band over time (blue circles) and fitting with the theoretical oxygen delivery equation (red) allows for the extraction of the time constant of delivery.

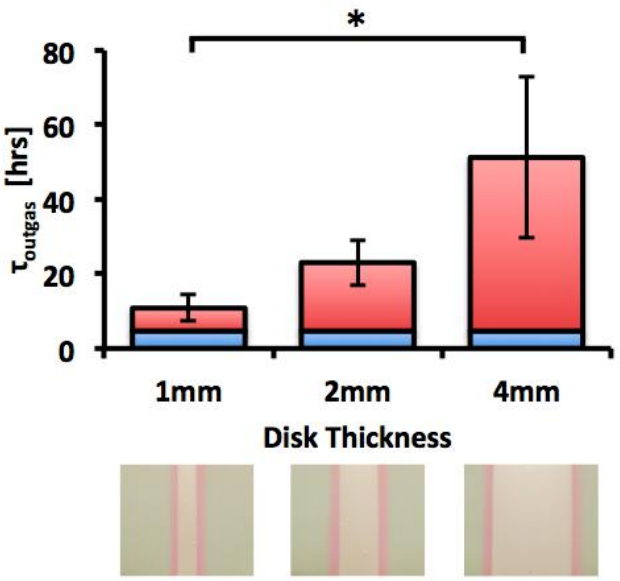

Figure III-5: Time constant of oxygen delivery increases with polymer thickness. Stacked bar graphs illustrate the contribution of the microtank (blue) vs bulk phase (red) time constants to the total outgassing time constant. Microtank filled PCL disk with thicknesses of 1mm, 2mm, and 4mm (pictured below in resazurin solution) were monitored over 1 week to extract time constants of delivery (above). N=3. * indicates significant difference ($P<0.05$ by one-way ANOVA and Tukey's HSD).

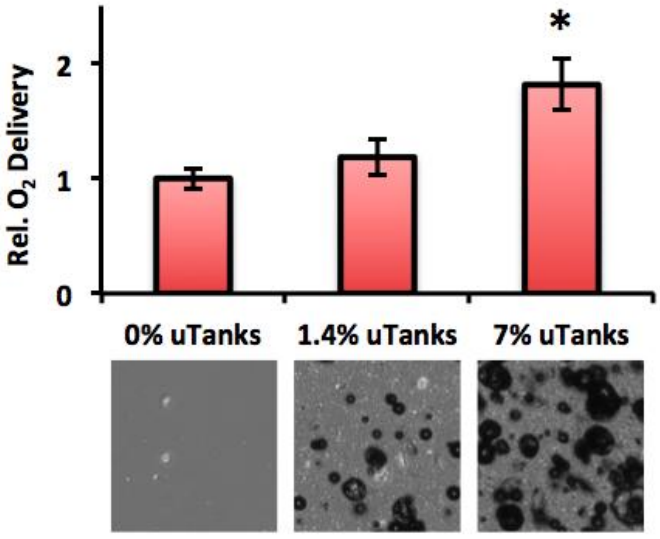

Figure III-6: Amount of oxygen delivery increases with microtank concentration. Plot of relative amount of oxygen released at 1hr time point from PCL disks containing 0, 1.4, or 7% V/V microtanks, normalized to pure PCL disk. N=3. * indicates significant difference ($P<0.05$ by one-way ANOVA and Tukey's HSD) between the 7% and the 0%, 1.4% groups.

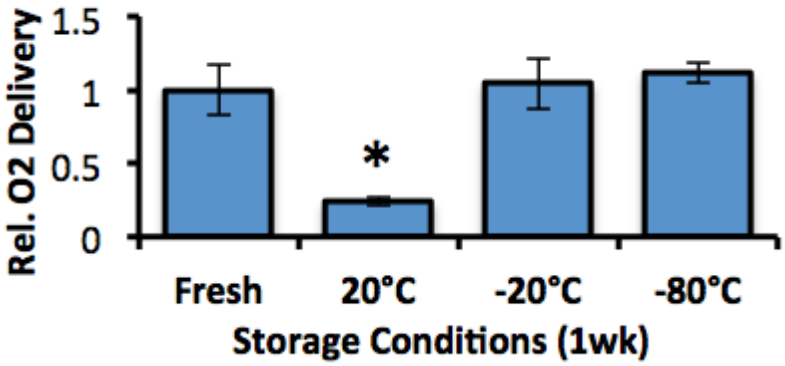

Figure III-7: Low temperatures enable storage of hyperbarically loaded scaffolds. Plot of relative amount of oxygen delivered at 1 hr time point from hyperbarically loaded PCL disks containing microtanks that were stored for 1 week in ambient pressure at 20°C, -20°C, or -80°C, normalized to disks stored under loading conditions in hyperbaric chamber. (N=2). * indicates significant difference (P<0.05 by one-way ANOVA and Tukey's HSD) from all other groups.

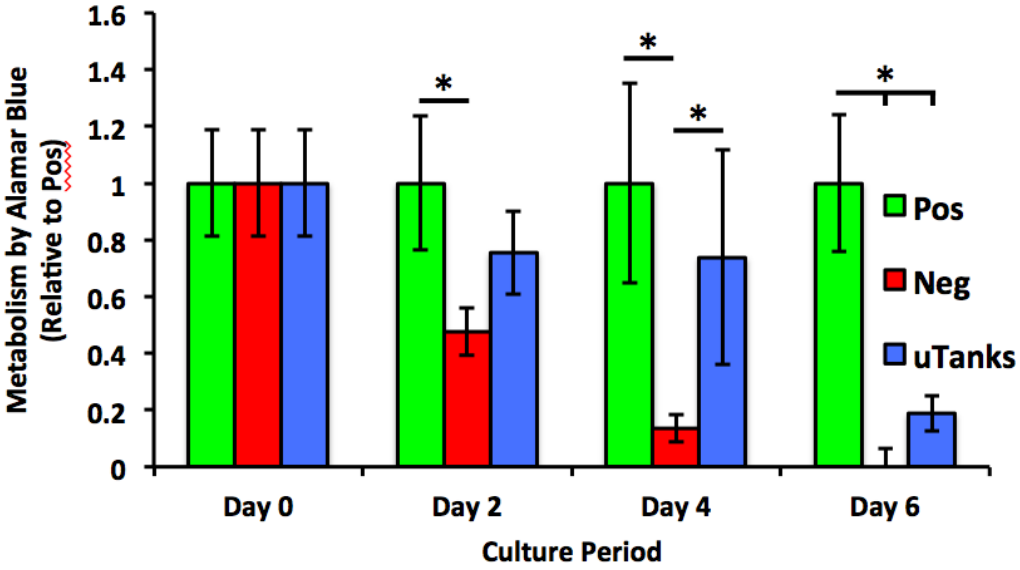

Figure III-8: Time course of ASC metabolism under anoxic conditions. Results of Alamar Blue assay of ASCs cultured in 3D fibrin gels on top of PCL disks containing oxygen loaded microtanks (uTanks), nitrogen purged microtanks (Neg), or ambient microtanks (Pos). uTank and Neg groups were cultured under anoxia (0% O_2, 5% CO_2, 95% N_2) while the Pos group was cultured under normoxia (21% O_2, 5% CO_2, 74% N_2). N=3. * indicates significant difference (P<0.05 by one-way ANOVA and Tukey's HSD) between indicated pairs.

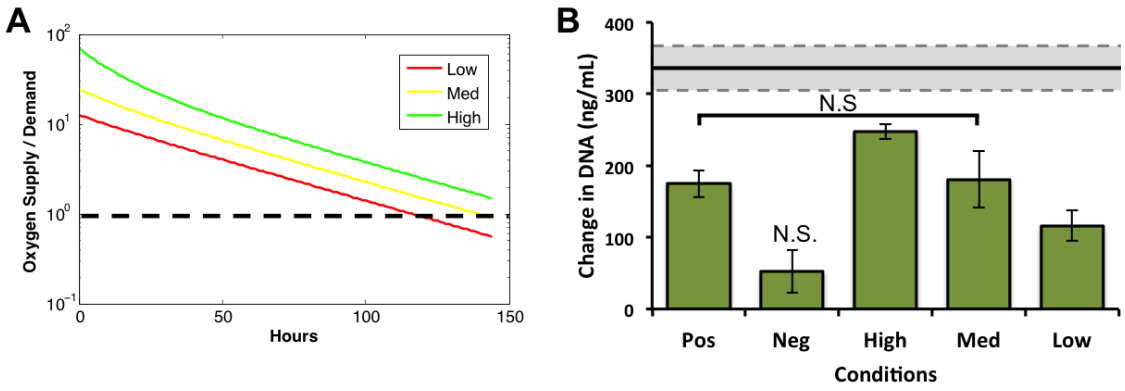

Figure III-9: Amount of oxygen delivery influences cellular growth. (A) Theoretical ratio of oxygen delivery from microtank loaded PCL disks to cellular demand over 6 day culture based on initial cell number, oxygen uptake rates from the literature, and measured delivery profiles. Disks were loaded with oxygen under the same conditions and pre-released for 3, 2, or 1 days before cell encapsulation in gel to achieve the high, medium, and low delivery profiles. Dashed line indicates threshold where delivery is equal to demand. (B) Change in DNA content by PicoGreen Assay within gels between Day 0 and 6 Days of anoxic culture (Neg, High, Med, Low) or normoxic culture (Pos). Black line indicates average growth in groups that received bi-daily feedings (dashed lines represent corresponding standard deviation); all other groups received only an initial 5mL of media. (N=4). All differences are statistically significant ($P<0.05$ by one-way ANOVA and Tukey's HSD), except Pos vs Med and Neg vs Day 0 as indicated by N.S.

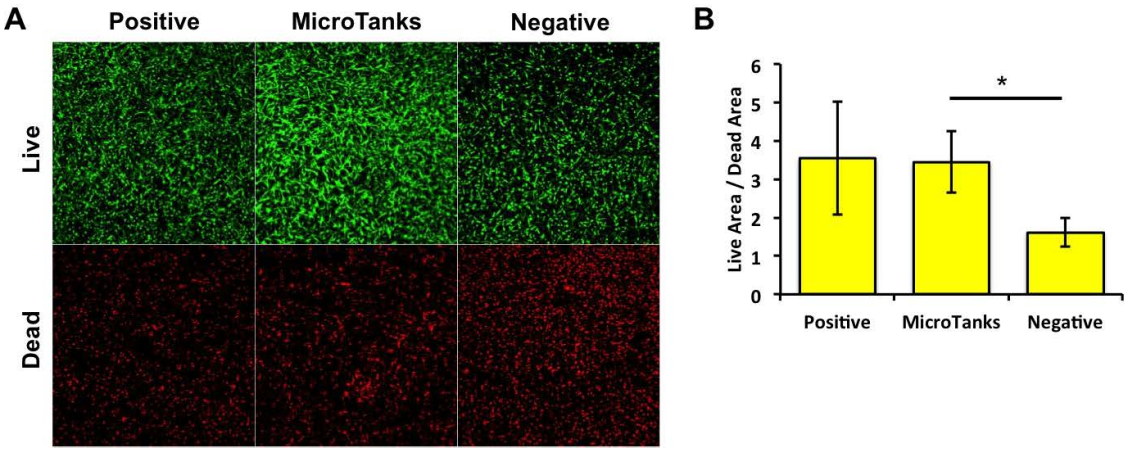

Figure III-10: Microtanks enhance vessel formation under anoxic conditions. (A) Confocal live (green) /dead (red) images (5x) of ASC:HUVECs in fibrin gels at Day 4. Representative images shown n=4. (B) Quantification of images using the ratio of areas of live and dead cells. * indicates significant difference by Student's t-test ($P<0.05$).

CHAPTER IV:

Translational Efforts and Applications

Development of standalone microtanks

From a translation perspective, it would be beneficial to formulate microtanks that possess the desired periods of release, biodegradable properties, and sufficient mechanical integrity to act as a stand-alone or additive component. The present implementation with microtanks embedded in PCL has potential utility within bone tissue engineering; however, the requirements of a structural phase limit the scope of application. The following will outline strategies and work done to extend the utility of the microtank approach for broader application.

Double emulsion approaches to engineer standalone microtanks

Double emulsions are a commonly utilized approach for forming microspheres and microcapsules[64]. Briefly, an aqueous phase containing the active compound is emulsified into an organic solvent phase containing the encapsulating polymer to form the primary water in oil emulsion (W/O). The primary emulsion is subsequently emulsified into an aqueous phase containing a surfactant, creating a water in oil in water double emulsion (W/O/W). The organic solvent is then evaporated causing the polymer to condense around the active compound. Thus microscopic, mono- or multi-core particles are formed[65]. Obviously, the

complimentary (O/W/O) double emulsion can be made too. Stir rates, evaporation rates, presence of surfactants, temperature, and viscosity can be varied to achieve different particle geometries.

Using a double emulsion approach, a strategy for forming biodegradeable, stand-alone microtanks was developed. The concept was to form a poly-lactic-glycolic acid polymer shell encapsulating a polyvinyl alchohol aqueous core, and subsequently evaporate off the water thus depositing the polyvinyl alcohol as an interior shell/coating. The PLGA outer shell is used for two purposes: firstly, it acts as a vapor barrier to protect the humidity sensitive PVA interior shell, and secondly, it acts to control the rate of degradation as the hydrolysis of PLGA can be easily tuned by changing the ratio of PLA:PGA of the polymer (PLA degrades much more slowly than PGA). The PVA interior shell acts as the oxygen barrier, the thickness of which controls the period of release from the microtank. As PVA is water soluble, once the PLGA shell biodegrades within the body the PVA is able to dissolve and be cleared from the body. Both PLGA and PVA are generally recognized as safe (**GRAS**) by the FDA.

A solution of 10% PVA in water was prepared by adding 10g of PVA into 100mL of water, bringing to a boil, and cooling to room temperature; Coomasie brilliant blue dye was added to better visualize the PVA phase. This acted as the first aqueous phase. A solution of 0.5% PVA was similarly prepared. This acted as the second aqueous phase. A solution of 0.5g PLGA was dissolved in 20mL of dichloromethane. This acted as the oil phase. 1mL of 10% PVA solution was emulsified in 20mL of the PLGA/dichloromethane phase by sonication at 10W for

30s. This emulsion was immediately poured into a 1000mL beaker containing 500mL of 0.5% PVA being stirred at 500rpm. The dichloromethane was allowed to evaporate overnight. The resulting particles were collected and washed 3x under distilled water.

Results:

Particles were imaged using bright field microscopy, shown in Figure IV-1**A,B**. Results indicated a mix of mono and multi-core particles with PLGA encapsulating a PVA aqueous core. Particle sizes ranged from 20-200um. Subsequently, particles were subject to drying under vacuum to drive off the water, shown in Figure IV-1**C**. The particles were found to be buoyant in water, indicating that they contained a hollow core.

To validate the formation of a PVA inner core, the PLGA outer core was dissolved away in dichloromethane. The resulting particles exhibited an approximately spherical geometry with visible lumen or hollow core as in Figure IV-1**D-G**. Buoyancy tests indicated that the particles were indeed hollow. These results suggest that the double emulsion approach is feasible for the formation of microtanks with appropriate geometry and biocompatible/biodegradable properties.

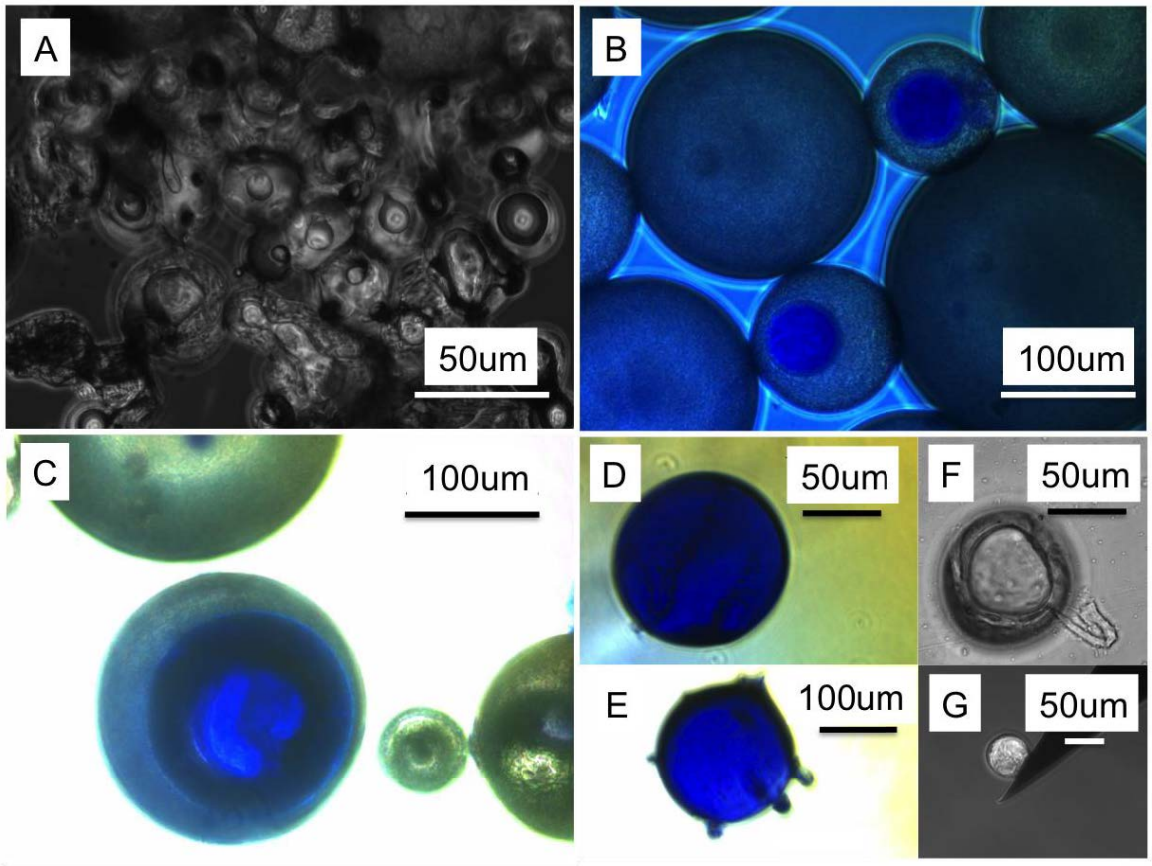

Figure IV-1: Bright field images of PLGA/PVA microtanks formed by double emulsion. (A, B) Core-shell morphology is apparent in many particles (C) Particles develop a darker colored shell surrounding the core following vacuum drying, indicating deposition of PVA around the interior surface (D, E) PVA microtanks are observed floating indicating they are indeed hollow. Approximately spherical geometries are obtained with some visible imperfections (F, G) PVA particle illustrating hollow core and subsequent manipulation on a needle tip.

Unfortunately, the double emulsion approach produces a distribution of particles and this is not desirable; however, the technique could be modified using microfluidic approaches to improve uniformity, reproducibility, and tunability. Of the numerous methods described within the literature for producing uniform mono-core capsules, droplet or capillary microfluidics appear to be the most promising for microtank fabrication. The system typically is composed of three phases (W/O/W) as illustrated in Figure IV-2[66]. Contrary to double emulsion approaches where

microcapsules are formed in two subsequent steps, within microfluidic approaches the microcapsules form in a single step as concentric streams of fluid pinch off into droplets. Based on the spatial organization of the system, it can be appreciated that the analogous primary emulsion is formed by injection of the inner aqueous phase into the dichloromethane/PLGA middle phase, and the analogous secondary emulsion is formed by injection of this concentric stream into the second aqueous outer phase. By varying the respective flow rates it is possible to generate microcapsules with a range of shell thicknesses and core diameters[67]. Evaporation of the aqueous core can transform the microcapsule into a microtank. Such an approach can be scaled up by utilizing massively parallel systems[68].

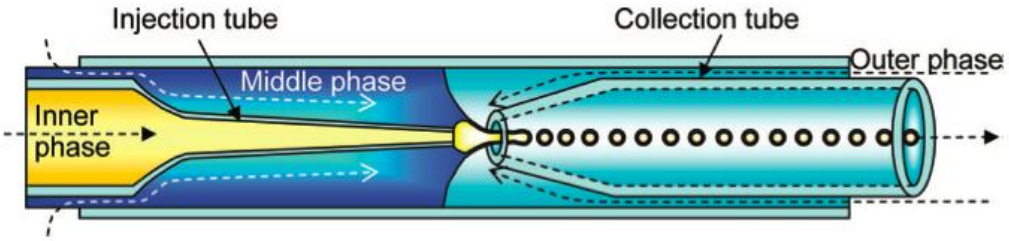

Figure IV-2: Capillary microfluidic approach to core-shell particle formation. The inner phase is injected through a concentric needle into the middle phase. These concentric streams are subsequently encapsulated by the outer phase and break up into droplets with a core-shell morphology. Varying the respective flow rates can alter the particle geometry and relative proportions of the shell and core. Reproduced from Shum, H. C. et al., 2008[66].

Interfacial polymerization approach, new chemistries, results

Interfacial polymerization is another approach commonly utilized in the formation of mono-core microcapsules, notably within the pesticides and pharmaceutical industry[69]. The approach relies on two complimentary monomers –

one monomer is soluble an aqueous phase and the other in an oil phase – which react with each other to form an insoluble polymer[70] as in Figure IV-3**A,B**. The compound to be encapsulated is dissolved in the desired phase and then emulsified to form microdroplets. The reactive monomers will meet at the liquid interface surrounding the droplet and begin developing a membrane, thus encapsulating the droplet. The advantage of interfacial polymerization is that encapsulation occurs in a single step and all particles are perfectly mono-core.

Commonly utilized monomer pairs are[71–73]: polyamine (PEI/TDC, SMA/polyamines, polyamine/polyuria, PEI/SC/TC/HAD, polyamide/polystyrene), polyurethane (IPDI/propanetriol, PU/poly(ether urethane), poly(ortho ester)/polyester, polyepoxide (EGDE/HMDA/DETA), polysiloxane (OES/TEOHS), polythiourea (TDITC/OPD), photo-cross-linking polyuria (polymeric isocyanate/polyamine), polyuria (MDI/HMDA/HMDI/DETA/polyamine, TDI/amines, nylon 6,10).

With consideration for biocompatibility and biodegradation, a new pair of monomers was investigated utilizing urethane chemistry. A urethane is most commonly formed by the reaction of an isocyanate (R–N=C=O) and an alcohol (R'-OH) to produce a urethane linkage (RNHCOOR'). Isocyanate can also react with itself in the presence of water to form a urea linkage (R-NH-CO-NH-R) and carbon dioxide gas. Polyurethane is thus formed by combining a di-/poly-isocyanate with a di-/poly-ol. In this study, PVA was utilized as both the polyol and the compound to encapsulate while HDMI was utilized as the diisocyanate, Figure IV-3**B**. Previous

studies seeking to modify PVA films had shown that the two would react to form a polyurethane[74,75].

Briefly, a solution of 10% PVA in water and a solution of 10% HDMI in toluene were made fresh. The PVA contained Coomasie brilliant blue for easy visualization. The PVA solution (5mL) was added to the HDMI solution and emulsified. The reaction was allowed to carry on over night. The following day, the particles were collected, washed under distilled water 3x, and imaged under bright field microscopy. Visual observations indicated that numerous microcapsules filled with blue PVA were formed as in Figure IV-3**C**. The microcapsules were resilient enough to be manipulated without rupturing. To the best of my knowledge, this represents the first time PVA microcapsules have been fabricated utilizing an interfacial polymerization approach.

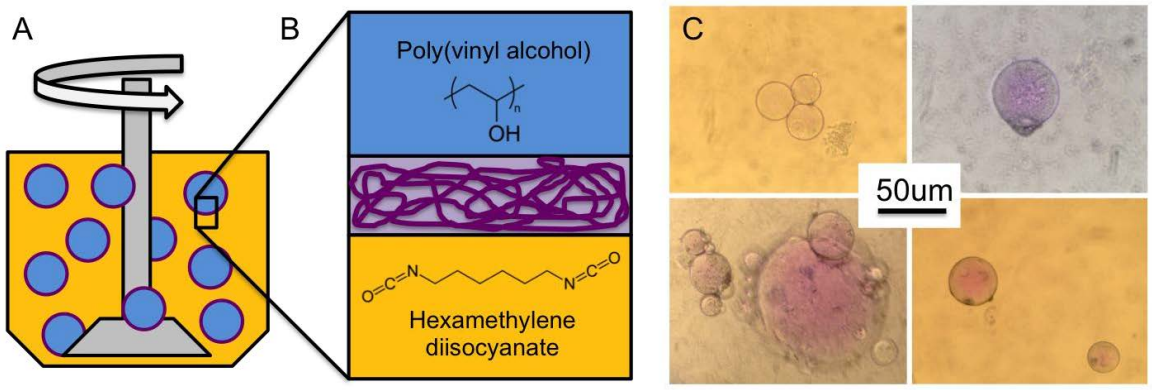

Figure IV-3: Interfacial polymerization approach yields monocore PVA filled microcapsule. (A) A single emulsion is formed with each phase containing a monomer reactive with the complimentary monomer in the opposite phase. At the interface where the monomers are able to meet, a urethane linkage forming reaction occurs producing a polymeric shell that encapsulates the dispersed phase. (B) Bright field microscope images of PVA filled microcapsules produced using this method.

Optimization of the polyurethane chemistry will need to be carried out to ensure the shell is mechanically rigid enough to support the subsequent evaporation of the aqueous core to coat the interior with a PVA shell. This may be accomplished by adding cross linkers to the aqueous phase such as glycerol to increase the rigidity of the polymer shell.

Simplicity by thoughtful reduction – Outgassing of polymeric foams

The generation of standalone microtanks represents a significant undertaking. Therefore, it is worth considering if the microtank concept can be simplified even more while maintaining the desired periods of release and oxygen capacity. Perhaps the most reduced implementation of the concept would be to use outgassing from hyperbarically loaded materials as a source of oxygen delivery. It is well established from the literature that many polymers have an intrinsic solubility for oxygen on the range of 5-10% V/V and tensile strengths on the order of 10-100MPa. Thus as an estimate for the upper limit of oxygen capacity of a hyperbarically loaded polymer, one could expect:

O_2 Capacity Hyperbarically Loaded Polymer:

$$C_{O_2} \approx \left(0.1 \frac{Vol.\ O_2}{Vol.\ Polymer}\right) \times (1000atm) \times \left(44.6 \times 10^{-6} \frac{mol\ O_2}{cm^3\ atm}\right) = 4.5\ molar\ O_2$$

(IV-1)

This is in comparison to the most oxygen dense alternative, calcium peroxide.

O_2 Capacity of Pure Calcium Peroxide:

$$C_{O_2} \approx \left(\frac{1\ mol\ O_2}{2\ mol\ CaO_2}\right) \times \left(2.91 \frac{g}{cm^3}\right) \times \left(72.1 \frac{g}{mol}\right) = 20\ molar\ O_2$$

(IV-2)

For a slightly more complicated system, a polymeric foam could be used where the polymer phase acts as both the walls of the microtanks as well as the structural component of the scaffold. This significantly increases the loading efficiency of the system. The oxygen capacity of the foam goes as:

$$\frac{Vol.\ O_2}{Vol.\ Polymer\ atm} = s\phi + (1 - \phi), where\ \phi = \frac{V_{polymer}}{V_{total}}$$

(IV-3)

Tensile Strength goes as:

$$\sigma_{foam} = \sigma \times \phi^{2/3}$$

(IV-4)

Thus, for the design of hyperbarically loaded polymeric foams, it is more favorable, from an oxygen content perspective, to increase void volume at the expense of maximum loading pressure. Obviously, the time constant of release also decreases as a function of void volume, so this consideration may impose a limit on void volume. A potentially interesting polymer to study from a biomedical perspective is

foamed PET as it provides high oxygen barrier, good biocompatibility, and comparable mechanical strength to bone.

Product design and applications

With tissue engineering likely decades away from becoming mainstream in the clinic, it is worthwhile to investigate existing applications that would benefit from oxygen delivery technology. A survey of the orthopedic market reveals a large number of polymeric implants that may be suitable for hyperbaric loading with oxygen. The local delivery of oxygen is anticipated to provide two primary therapeutic roles: firstly, preventing infections by increasing the leukocyte respiratory burst, and secondly, enhancing the rate of healing through increased production of collagen. For applications such as medical fasteners, these two properties are very desirable. Figure IV-4 illustrates several of such applications; stiches are another potential application. In many cases the fasteners are made from nylon, PEEK, or PET which have sufficient oxygen barrier properties to afford a period of oxygen release out to two or three weeks. The appeal of such applications is that the products already exist, have defined markets, and known utility; thus, the oxygen delivery component becomes an additive technology to improve health outcomes.

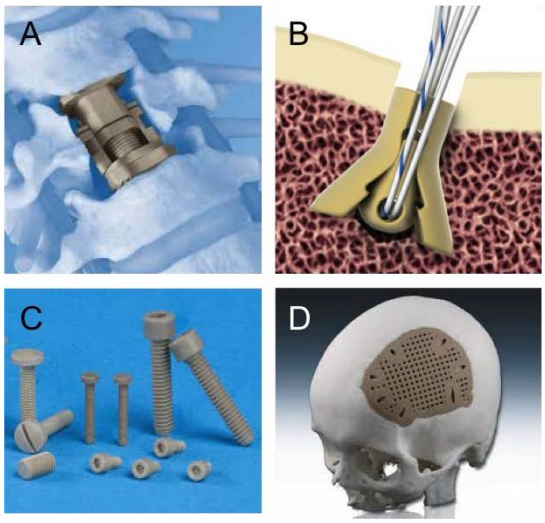

Figure IV-4: Existing medical applications may benefit from hyperbaric oxygen loading and delivery. (A) Spinal fusion cages (B) Suture anchors (C) Medical fasteners and screws (D) PEEK implants

Potential Synergy with Dimethyloxaloylglycine HIF-1α

There are legitimate concerns that within certain applications, the delivery of oxygen may suppress the beneficial effects of HIF-1α signaling, which is known to enhance blood vessel recruitment through upregulated VEGF secretion. However, by pretreating cells or delivering the small molecule upregulator of HIF-1 α, dimethyloxaloylglycine, it may be possible to induce a beneficial hypoxic response without incurring the negative consequences of chronic hypoxia. Dimethyloxaloylglycine works by inhibiting PHD[76] and FIH-1[77], which are known inhibitors of the HIF-1α pathway. When combined with oxygen delivery technology, such as microtanks, the approach could achieve synergy by tricking cells into thinking they are hypoxic yet providing the necessary oxygen for metabolic function and ECM deposition.

CHAPTER V:

Commercialization and Translation Strategy

Defining Target Markets

Clinical translation requires a defined, substantial market as well as a developed technology. Therefore, in developing a commercial strategy for the technology presented within this thesis, one must be cognizant of the present and future markets for oxygen delivery as well as the present state and anticipated developments of the microtank technology. Figure V-1 summarizes the following analysis.

The hyperbaric loading of materials with oxygen represents a novel oxygen delivery approach. The approach can be implemented in two distinct ways: the controlled outgassing of bulk & foamed polymers or from the controlled release of gas from stand-alone microtanks. From a technology development perspective, the outgassing of bulk & foamed polymers is far more developed, and technologically simpler, than the standalone microtanks. Outgassing of bulk polymers & foams has application in at least two distinct markets: the medical fastener and the orthopedic scaffold market. Of these, the medical fastener market is better established and presents an easier pathway to entry. Regarding the markets for stand-alone microtanks, there are applications in wound care and graft management as well as within tissue engineering. The market for wound care and graft management is very well established, growing, and would be highly receptive to an oxygen delivery technology. The tissue engineering market is primarily academic in nature and expected to remain so for the next decade. Therefore, from a translation

perspective the most immediate market to target is the medical fasteners market. The wound care and the graft management markets also represent a very appealing space to enter, but will require further development of stand-alone microtanks. Emphasis will be placed on these two markets as immediate and future prospects, given that the tissue engineering market will require significant time to develop.

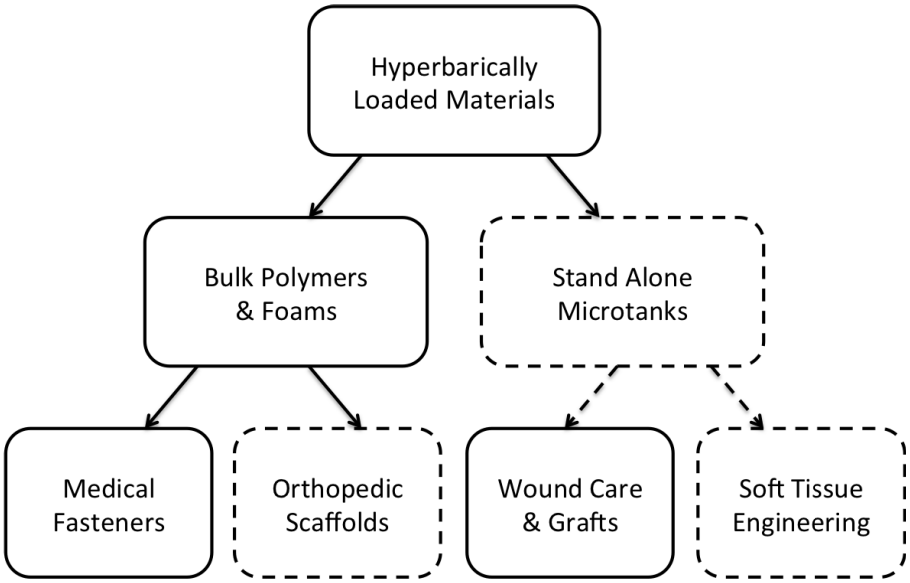

Figure V-1: Pathways from technology to markets. Solid lines indicate technology / markets that exist today where as dashed lines indicate technology / markets in development. Medical fasteners and wound care represent the most immediate markets to target.

Medical Fasteners

The delivery of oxygen is known to enhance collagen deposition, prevent infection, and enhance vasculogenesis. From a biomedical perspective, these would be excellent properties to incorporate into various medical fasteners. A medical fastener is a device which secures, anchors, attaches, or otherwise interfaces with tissue and/or an implanted material: examples include, screws, suture anchors, stiches, foils, plates,

meshes, tapes, and prosthetic ligaments. Medical fasteners inherently cause local damage to the tissue during installation including the disruption of local blood supply, volumetric bone loss, and occasionally fracture. Two of the most common failure modes for medical fasteners are infection and pullout. From a therapeutic perspective, oxygen delivery would be beneficial in that the increased collagen deposition would mitigate pullout and the enhanced antimicrobial properties would moderate infection.

Many medical fasters are now available in polymeric versions, which have the advantage of being imaging compatible compared to metallic versions, with some even bioresorbable. A survey of medical fasteners indicates a large number are fabricated out of polymers suitable for hyperbaric loading with oxygen, namely: polyethylene terephthalate (meshes, suture, vascular grafts), polyether ether ketone (suture anchors, interference screws, spinal cages, disc arthroplasty, craniofacial implants), polyamide (sutures, meshes, foil), and recently polylactide (bioresorbable screws, plates, scaffolds). As can be quickly estimated from the graph in Figure V-2, if medical fasteners were hyperbarically loaded with oxygen they would be expected to deliver oxygen over a period of hours to weeks depending on their geometry.

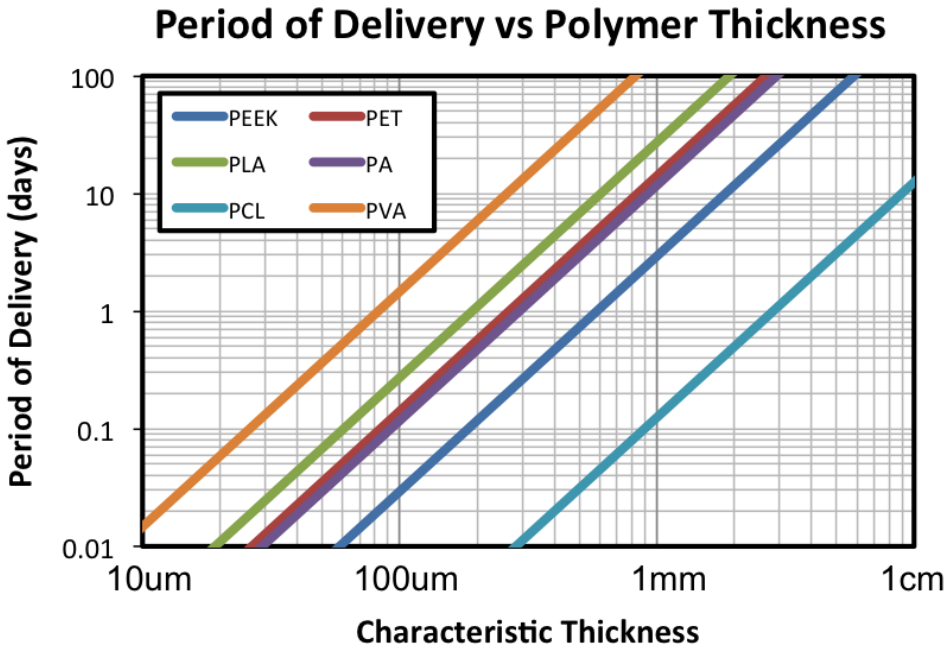

Figure V-2: Oxygen delivery periods of commonly used medical polymers. The time constant of oxygen delivery from an existing medical fastener, implant, or device can be easily estimated from this chart if the polymer and characteristic thickness are known.

Suture Anchors

Suture anchors are devices that screw into the bone to provide fastening points for sutures, which commonly connect to soft tissue like ligament or tendon. Consider for example the Smith and Nephew PEEK Suture Anchors, which have a diameter of 2-3mm, depicted in Figure V-3. If hyperbarically loaded with oxygen, one would expect a time constant of oxygen delivery on the order of 1 week. Polylactide versions might delivery oxygen over a period of several weeks.

Suture anchors typically cost around $250 each[78] and several are used within each surgery. For example, the repair of a ruptured quadricep tendon involves 3 anchors; an arthroscopic shoulder stabilization procedure will involve at least 3 suture anchors[79,80].

Surgeon are increasingly favoring the use of polymer suture anchors, especially PLA models due to their bioresorbable properties. The current 2014 market fixation systems for cartilage and soft tissue is estimated at $1.4 billion[81], accounting for 75% of the soft tissue repair and regenerative product market. It has been growing at a rate of 6% per year over the past 4 years driven by favorable demographics and the prevalence of sports-related injuries.

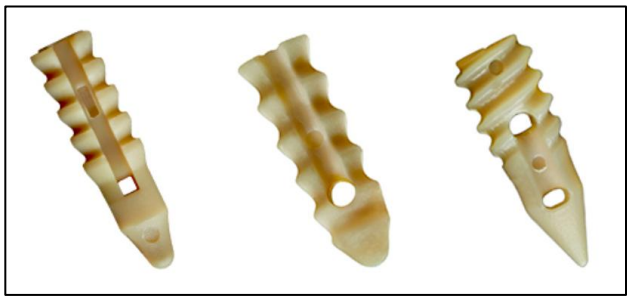

Figure V-3: Smith and Nephew PEEK polymer suture anchors. (L-R) Raptormite, Dynomite, Spyromite models. Diameters are 3mm, 2mm, 2mm, respectively.

Other Applications

Nylon foil (0.4mm thick nylon sheet) is commonly used in the repair of pediatric orbital wall fracture [82] and could benefit from hyperic loading**.** Other applications that may benefit from hyperbaric loading with oxygen are[83,84]: transcatheter aortic-valve implantation, transcatheter aortic-valve replacement, aortic heart valve sewing rings, aortic heart valve fabric, mitral valve components, annuloplasty rings, cardiovascular patches, embolic protection devices, vascular grafts, coronary artery bypass grafts, stent grafts, tapered endovascular grafts, endovascular aneurysm repair, thoracic endovascular aneurysm repair, abdominal aortic aneurysm stent grafts, thoracic aortic aneurysm stent

grafts, bifurcated endovascular grafts, vascular grafts, embolic protection devices, artificial ligaments, artificial tendons, long bone fixation devices, spinal stabilization, containment devices, tethers, prosthetic ligaments, pelvic floor repair mesh, incontinence slings, hernia mesh, prolapse repair slings, surgical mesh, abdominal wall patches, nerve regeneration conduits/ tubes, tissue engineering scaffolds, bio-absorbable scaffolds, stem cell platforms, bio-absorbable meshes, hybrid medical fabrics, hernia mesh, surgical mesh, abdominal wall patches, breast lift slings, cosmetic surgical mesh, and sutures.

Entry Strategy into Medical Fasteners

Consequently, the medical fastener market represents a particularly unique opportunity for entry. There are two obvious means of monetizing this technology. Firstly, the patented outgassing technology could be licensed directly to the manufacturers of these products for hyperbaric loading in-house. This is the simplest approach and has the advantage of utilizing the established sales network and manufacturing facilities of the company. From the perspective of the company, the licensing of the oxygen outgassing technology is beneficial because it allows them to differentiate their products from others in a very crowded and stagnant market[81]. The therapeutic benefit of the oxygen makes the pitch to hospitals, clinicians, and patients a more tractable one and may allow a premium to be charged.

From a licensing perspective, the larger players provide the best opportunity due to their broader product lines, R&D budgets, and sales volume. The major players within the medical fasteners market are:

1. **Smith and Nephew** – The leading provider of soft tissue and cartilage repair products with 22% marketshare (revenues $405 million in 2014). Has substantial offerings including anchor systems for shoulder repair, soft tissue repair products for the knees and other-extremity soft tissue repair products. S&N's strong track record in the orthopedic industry, together with substantial R&D resourses, are predicted to play a major role in its continued success.

2. **Arthrex** – The second largest player, advancing recently to become a top tier provider, with a market share of 22% (revenues $400 million in 2014). It specializes in the area of tendon repair, rotator cuff repair, ligament reconstruction, meniscal fixation and transplant as well as other areas of the cartilage and soft tissue market.

3. **Johnson & Johnson / DePuy** – Holds the third spot with a marketshare of 12% (revenues of $220 million in 2014). It caters to cartilage repair, meniscal repair and soft tissue biological implants. DePuy's comprehensive product line is predicted to provide an opportunity for future market leadership.

4. **Biomet** – With a market share of 10% (revenues of $180 million) ranks fourth. Its primary strength is in the fixation device segment.

Industry reports indicate that the most significant factors increasing market position are[81,85]:

- Product cost and price
- Product design, quality and ease of use
- **Improved patient outcomes**
- Increasing surgeon and physician acceptance
- Distribution capabilities
- **Patent protection**
- **New product innovation timing and market**

Thus hyperbaric outgassing technology makes good strategic sense for these companies. Additionally, many of these companies have several divisions that could make similar use of the technology.

The second approach is to setup a hyperbaric loading company, which would charge companies, hospitals, or clinicians a fee for the functionalization of their implants. This approach faces logistical complications, as it would require inserting another node within the supply chain. It is not a favorable option.

Wound Care & Graft Management

The wound care market is a four-tiered market dominated by three major players (Johnson and Johnson, Smith and Nephew, and 3M)[86] who have been making large acquisitions over the past decade, significantly consolidating the market. It includes wound dressings, skin replacements, and the like. Acquisitions have primarily involved smaller firms with strong R&D pipelines but relatively weak distribution networks. The advanced wound care market is valued at $11.3B in 2013[87] with wound dressings accounting for 55% of this market. The trend within the market is a move away from dry

dressings towards moist dressings, which are demonstrating enhanced wound healing. The major limitation facing companies within the market is the inability to distinguish their products from competitors' products. This has led to efforts to functionalize wound dressings with additional features, such as silver particles for antimicrobial properties, but there has been a dearth of further meaningful adjuncts to dates.

One of the popular adjunctive therapies utilized for advanced wound healing is hyperbaric oxygen therapy. Hyperbaric oxygen has been shown to increase healing outcomes by 80% through reduced infection, increased vascularization, and tissue remodeling. The size of the hyperbaric oxygen market was estimated to be $140 million in 2000[37], however growth was limited by Medicare approved indications. Furthermore, the treatment requires the patient to make daily visits to a center, which is time consuming and inconvenient. In the 2000 Frost and Sullivan report "Impact of Hyperbaric Oxygen Therapy on the U. S. Wound Care Industry" analysts identified hyperbaric oxygen therapy to play a major role in the care of diabetic ulcers, an indication not yet approved by Medicare. Estimates were that the beneficial effects of hyperbaric oxygen applied to the 2006 diabetic foot ulcer market could have had potential health savings of $1.4 billion/year. The failure for hyperbaric oxygen therapy to become widely adopted despite growing evidence of its benefit is largely due to the method of delivery. A means of locally delivering oxygen to a wound without the need for repeat trips to a clinic would likely encourage healthcare providers to utilize adjunctive oxygen therapy.

The development of standalone microtanks that could provide a local supply of oxygen to a wound environment would therefore represent a great advance within wound

care management. Microtanks could provide both enhanced therapeutic outcomes but also a means by which a wound dressing brand could stand out in a crowded market, thus meeting the present demands of the market. Hyperbaric therapy currently costs between $10,000-40,000 for a course of treatment, giving an indication of the value of the therapeutic effect. If local delivery of oxygen by microtanks could provide a comparable therapeutic benefit, a large premium could be charged.

Stand alone microtanks would also find a market in the field of plastic surgery where transplanted grafts are routinely compromised due to local hypoxia as the blood supply has been interrupted. The injection of microtanks throughout the graft or coating on the surfaces in the case of thin grafts (e.g. skin) could help to mitigate this complication. Finally, tissue engineering R&D will remain a small but nontrivial market for oxygen delivery technology. R&D applications are advantageous as they provide a source of early cash flow without needing to go through the arduous FDA-approval process. It is almost certain that if cellularized scaffolds are used within tissue engineering, some form of initial oxygen and nutrient augmentation will be required. Hopefully, microtanks can fill this niche.

Entry Strategy into Wound Care

As a standalone product, microtanks are ideal for a startup company, which can produce and initially sell the microtanks directly to researchers interested in combining oxygen delivery technology with their current work (e.g. tissue engineering, wound repair, transplantation). This beta-testing period will allow sufficient evidence of safety and efficacy to be collected to apply for FDA-approval, either directly or by licensing the

technology to a larger company. The manufacturing costs associated with microtank fabrication, assuming microfluidic approaches are used, are manageable for a small company. Furthermore, there exists a range of intermediate production options to facilitate scale up.

Intellectual Property Protection

Two provisional patent applications were filed with the United States Patent and Trademark Office to cover the technology and applications described within this document in May, 2013. These have both been converted into Patent Cooperation Treaty international patent applications.

REFERENCES

1. De Groot, M., Schuurs, T. a & van Schilfgaarde, R. Causes of limited survival of microencapsulated pancreatic islet grafts. *J. Surg. Res.* **121,** 141–50 (2004).

2. Khattak, S. F., Chin, K., Bhatia, S. R. & Roberts, S. C. Enhancing Oxygen Tension and Cellular Function in Alginate Cell Encapsulation Devices Through the Use of Perfluorocarbons. **96,** 156–166 (2007).

3. Malda, J. *et al.* Oxygen gradients in tissue-engineered PEGT/PBT cartilaginous constructs: measurement and modeling. *Biotechnol. Bioeng.* **86,** 9–18 (2004).

4. Chen, J. *et al.* In vivo chondrogenesis of adult bone-marrow-derived autologous mesenchymal stem cells. *Cell Tissue Res.* **319,** 429–38 (2005).

5. Moon, J. J. & West, J. L. Vascularization of Engineered Tissues - Approaches to Promote Angiogenesis in Biomaterials. *NIH Public Access* **8,** 300–310 (2014).

6. Malda, J., Klein, T. J. & Upton, Z. The roles of hypoxia in the in vitro engineering of tissues. *Tissue Eng.* **13,** 2153–62 (2007).

7. Zhu, W., Chen, J., Cong, X., Hu, S. & Chen, X. Hypoxia and serum deprivation-induced apoptosis in mesenchymal stem cells. *Stem Cells* **24,** 416–25 (2006).

8. Koh, M. Y. & Powis, G. Passing the baton: the HIF switch. *Trends Biochem. Sci.* **37,** 364–72 (2012).

9. Ehsan, S. M. & George, S. C. Nonsteady State Oxygen Transport in Engineered Tissue : Implications for Design. **19,** (2013).

10. Semenza, G. L. Regulation of mammalian oxygen homeostasis by hypoxia-inducible factor 1. *Annu. Rev. Cell Dev. Biol.* **15,** 551–578 (1999).

11. Stoppel, W. L. & Roberts, S. C. *Engineering Biomaterials for Regenerative Medicine*. (Springer New York, 2012). doi:10.1007/978-1-4614-1080-5

12. Croll, T. I. *et al.* Modelling oxygen diffusion and cell growth in a porous, vascularising scaffold for soft tissue engineering applications. *Chem. Eng. Sci.* **60,** 4924–4934 (2005).

13. Spencer, J. a *et al.* Direct measurement of local oxygen concentration in the bone marrow of live animals. *Nature* **508,** 269–73 (2014).

14. Winegrad, S., Henrion, D., Rappaport, L. & Samuel, J. L. Self-Protection by Cardiac Myocytes Against Hypoxia and Hyperoxia. *Circ. Res.* **85,** 690–698 (1999).

15. Wang, G. L. & Semenza, G. L. General involvement of hypoxia-inducible factor 1 in transcriptional response to hypoxia. **90,** 4304–4308 (1993).

16. Utting, J. C. *et al.* Hypoxia inhibits the growth, differentiation and bone-forming capacity of rat osteoblasts. *Exp. Cell Res.* **312,** 1693–702 (2006).

17. D'Ippolito, G., Diabira, S., Howard, G. a, Roos, B. a & Schiller, P. C. Low oxygen tension inhibits osteogenic differentiation and enhances stemness of human MIAMI cells. *Bone* **39,** 513–22 (2006).

18. BASSETT, C. A. L. & HERRMANN, I. Influence of Oxygen Concentration and Mechanical Factors on Differentiation of Connective Tissues in vitro. *Nature* **190,** 460–461 (1961).

19. Kourembanas, S., Hannan, R. L. & Faller, D. V. Oxygen tension regulates the expression of the platelet-derived growth factor-B chain gene in human endothelial cells. *J. Clin. Invest.* **86,** 670–4 (1990).

20. Forsythe, J. A. *et al.* Activation of vascular endothelial growth factor gene transcription by hypoxia-inducible factor Activation of Vascular Endothelial Growth Factor Gene Transcription by Hypoxia-Inducible Factor 1. *Mol. Cell. Biol.* (1996).

21. Falanga, V. *et al.* Hypoxia Upregulates the Synthesis of TGF-beta1 by Human Dermal Fibroblasts. *J. Invest. Dermatol.* **97,** 634–637 (1991).

22. Albina, J. E. *et al.* HIF-1 expression in healing wounds: HIF-1alpha induction in primary inflammatory cells by TNF-alpha. *Am. J. Physiol. Cell Physiol.* **281,** C1971–7 (2001).

23. Siddiqui, A. *et al.* Differential effects of oxygen on human dermal fibroblasts: acute versus chronic hypoxia. *Wound Repair Regen.* **4,** 211–8

24. Löndahl, M. Hyperbaric oxygen therapy as adjunctive treatment of diabetic foot ulcers. *Med. Clin. North Am.* **97,** 957–80 (2013).

25. Tandara, A. a & Mustoe, T. a. Oxygen in wound healing--more than a nutrient. *World J. Surg.* **28,** 294–300 (2004).

26. Daniel, B. *et al.* Wound Hypoxia and Acidosis Limit Neutrophil Bacterial Killing Mechanism. *Arch. Surg.* **132,** 991–996 (1997).

27. Velazquez, O. C. Angiogenesis and vasculogenesis: inducing the growth of new blood vessels and wound healing by stimulation of bone marrow-derived progenitor cell mobilization and homing. *J. Vasc. Surg.* **45 Suppl A,** A39–47 (2007).

28. Sheikh, a Y. *et al.* Effect of hyperoxia on vascular endothelial growth factor levels in a wound model. *Arch. Surg.* **135,** 1293–7 (2000).

29. Sheikh, A. Y., Rollins, M. D., Hopf, H. W. & Hunt, T. K. Hyperoxia improves microvascular perfusion in a murine wound model. *Wound Repair Regen.* **13,** 303–8 (2005).

30. Castro, C. I. & Briceno, J. C. Perfluorocarbon-based oxygen carriers: review of products and trials. *Artif. Organs* **34,** 622–34 (2010).

31. Tamimi, F. *et al.* Perfluorodecalin and bone regeneration. *Eur. Cell. Mater.* **25,** 22–36 (2013).

32. Radisic, M. *et al.* Biomimetic approach to cardiac tissue engineering: oxygen carriers and channeled scaffolds. *Tissue Eng.* **12,** 2077–91 (2006).

33. Kimelman-Bleich, N. *et al.* The use of a synthetic oxygen carrier-enriched hydrogel to enhance mesenchymal stem cell-based bone formation in vivo. *Biomaterials* **30,** 4639–48 (2009).

34. Ma, Y., Zhang, B., Zhao, L., Guo, G. & Lin, J. Study on the generation mechanism of reactive oxygen species on calcium peroxide by chemiluminescence and UV-visible spectra. 575–580 (2007). doi:10.1002/bio

35. Oh, S. H., Ward, C. L., Atala, A., Yoo, J. J. & Harrison, B. S. Oxygen generating scaffolds for enhancing engineered tissue survival. *Biomaterials* **30,** 757–62 (2009).

36. Camci-Unal, G., Alemdar, N., Annabi, N. & Khademhosseini, A. Oxygen Releasing Biomaterials for Tissue Engineering. *Polym. Int.* **62,** 843–848 (2013).

37. Frost and Sullivan. *Impact of Hyperbaric Oxygen Therapy on the U . S . Wound Care Industry*. 1–107 (2000).

38. Spiess, B. D. Perfluorocarbon emulsions as a promising technology: a review of tissue and vascular gas dynamics. *J. Appl. Physiol.* **106,** 1444–52 (2009).

39. Eggleton, C. D., Roy, T. K. & Popel, a S. Predictions of capillary oxygen transport in the presence of fluorocarbon additives. *Am. J. Physiol.* **275,** H2250–7 (1998).

40. Harrison, B. S., Eberli, D., Lee, S. J., Atala, A. & Yoo, J. J. Oxygen producing biomaterials for tissue regeneration. *Biomaterials* **28,** 4628–34 (2007).

41. Winterbourn, C. C. Reconciling the chemistry and biology of reactive oxygen species. *Nat. Chem. Biol.* **4,** 278–86 (2008).

42. Wang, J. *et al.* Oxygen-generating nanofiber cell scaffolds with antimicrobial properties. *ACS Appl. Mater. Interfaces* **3,** 67–73 (2011).

43. Hunt, T. K., Niinikoski, J. & Zederfeldt, B. Role of oxygen in repair processes. *Acta Chir. Scand.* **138,** 109–10 (1972).

44. Prockop, D. J., Kivirikko, K. I., Tuderman, L. & Guzman, N. A. The biosynthesis of collagen and its disorders (first of two parts). *N. Engl. J. Med.* **301,** 13–23 (1979).

45. Chambers, a C. & Leaper, D. J. Role of oxygen in wound healing: a review of evidence. *J. Wound Care* **20,** 160–4 (2011).

46. Wattel, F. & Wattel, F. Acute peripheral ischaemia and compartment syndromes: A role for hyperbaric oxygenation. *Anaesth. Suppl.* **53,** 63 – 65 (1998).

47. Thom, S. R. *et al.* Regulation and Function of Stem Cells in the Cardiovascular System Stem cell mobilization by hyperbaric oxygen. 1378–1386 (2006). doi:10.1152/ajpheart.00888.2005.

48. Kang, T. S., Gorti, G. K., Quan, S. Y., Ho, M. & Koch, R. J. Effect of hyperbaric oxygen on the growth factor profile of fibroblasts. *Arch. Facial Plast. Surg.* **6,** 31–5 (2014).

49. Bonomo, S. R. *et al.* Hyperbaric oxygen as a signal transducer: upregulation of platelet derived growth factor-beta receptor in the presence of HBO2 and PDGF. *Undersea Hyperb. Med.* **25,** 211–6 (1998).

50. Ward, C. L., Haines, N., Patel, R., Eisele, E. & Harrison, B. S. Assessing angiogenic activity of cells in the presence of oxygen generating biomaterials. *FASEB J* **23,** 951.8– (2009).

51. Koros, W. J. Polymeric gas separation membranes. By R. E. Kesting and A. K. Fritzsche, Wiley Interscience Publishers, New York, 1993, XI+ 416 pp. *AIChE J.* **40,** 1925–1926 (1994).

52. Chiou, J. S. & Paul, D. R. Gas transport in a thermotropic liquid-crystalline polyester. *J. Polym. Sci. Part B Polym. Phys.* **25,** 1699–1707 (1987).

53. Segovia, J. L. De. *PHYSICS OF OUTGASSING*. 99–110

54. Brody, R., Brody, A. L. & Ph, D. A TWENTY-YEAR RETROSPECTIVE ON PLASTICS : OXYGEN BARRIER PACKAGING MATERIALS Gene Strupinsky.

55. Siracusa, V. Food Packaging Permeability Behaviour: A Report. *Int. J. Polym. Sci.* **2012,** 1–11 (2012).

56. Kuraray. *EVAL* ^{TM} *, a unique Kuraray technology*. *Tech. Broch.* (2013).

57. Crank, J. *The Mathematics of Diffusion*. 47–48 (Oxford University Press, 1975).

58. Ghosal, K. & Freeman, B. D. Gas separation using polymer membranes: an overview. *Polym. Adv. Technol.* **5,** 673–697 (1994).

59. Vieth, W. & Wuerth, W. F. Transport properties and their correlation with the morphology of thermally conditioned polypropylene. *J. Appl. Polym. Sci.* **13,** 685–712 (1969).

60. Bitter, J. G. A. Effect of crystallinity and swelling on the permeability and selectivity of polymer membranes. *Desalination* **51,** 19–35 (1984).

61. Crompton, T. R. *Physical Testing of Plastics*. 1–148 (Smithers Rapra Technology, 2012).

62. Von Heimburg, D., Hemmrich, K., Zachariah, S., Staiger, H. & Pallua, N. Oxygen consumption in undifferentiated versus differentiated adipogenic mesenchymal precursor cells. *Respir. Physiol. Neurobiol.* **146,** 107–16 (2005).

63. Eberl, T. & Gnaiger, E. Oxygen dependence of respiration and uncoupled endothelial cells in coupled.

64. Datta, S. S. *et al.* 25Th Anniversary Article: Double Emulsion Templated Solid Microcapsules: Mechanics and Controlled Release. *Adv. Mater.* **26,** 2205–18 (2014).

65. Dubey, R., Shami, T. C. & Rao, K. U. B. Microencapsulation Technology and Applications. **59,** 82–95 (2009).

66. Shum, H. C., Kim, J.-W. & Weitz, D. a. Microfluidic fabrication of monodisperse biocompatible and biodegradable polymersomes with controlled permeability. *J. Am. Chem. Soc.* **130,** 9543–9 (2008).

67. Tu, F. & Lee, D. Controlling the stability and size of double-emulsion-templated poly(lactic-co-glycolic) acid microcapsules. *Langmuir* **28,** 9944–52 (2012).

68. Romanowsky, M. B., Abate, A. R., Rotem, A., Holtze, C. & Weitz, D. a. High throughput production of single core double emulsions in a parallelized microfluidic device. *Lab Chip* **12,** 802–7 (2012).

69. Lee, M. H. *et al.* Harnessing Interfacial Phenomena to Program the Release Properties of Hollow Microcapsules. *Adv. Funct. Mater.* **22,** 131–138 (2012).

70. Crotts, G. & Park, T. G. Preparation of porous and nonporous biodegradable polymeric hollow microspheres. *J. Control. Release* **35,** 91–105 (1995).

71. Re, Y. F. R. E., Danicher, L. & Gramain, P. Preparation of polyurethane microcapsules by interfacial polycondensation. **34,** 193–199 (1998).

72. Pharmacotechnie, L. De, Pharmacie, F. De, Pharmacotcchnie, D. & Pharmacie, D. Microcapsules prepared through interfacial cross-linking of starch derivatives. **62,** (1990).

73. Zhang, Y. & Rochefort, D. Characterisation and applications of microcapsules obtained by interfacial polycondensation. *J. Microencapsul.* **29,** 636–49 (2012).

74. Caro, S. V, Sung, C. S. P. & Merrill, E. W. Reaction of Hexamethylene Diisocyanate with Poly (vinyl Alcohol) Films for Biomedical Applications. **20,** 3241–3246 (1976).

75. Giménez, V., Mantecón, A. & Cádiz, V. Modification of poly(vinyl alcohol) with acid chlorides and crosslinking with difunctional hardeners. *J. Polym. Sci. Part A Polym. Chem.* **34,** 925–934 (1996).

76. Rabinowitz, M. H. Inhibition of hypoxia-inducible factor prolyl hydroxylase domain oxygen sensors: tricking the body into mounting orchestrated survival and repair responses. *J. Med. Chem.* **56,** 9369–402 (2013).

77. Mahon, P. C., Hirota, K. & Semenza, G. L. FIH-1: a novel protein that interacts with HIF-1alpha and VHL to mediate repression of HIF-1 transcriptional activity. *Genes Dev.* **15,** 2675–86 (2001).

78. HR, L. W. C. D. L. R. P. B. B. H. Tunnel Fixation for Quadriceps Tendon Rupture : A Biomechanical Study. *Orthopedics* **31,** (2008).

79. Ozbaydar, M., Elhassan, B. & Warner, J. J. P. The use of anchors in shoulder surgery: a shift from metallic to bioabsorbable anchors. *Arthroscopy* **23,** 1124–6 (2007).

80. Cole, B. J. & Romeo, A. A. Arthroscopic Shoulder Stabilization With Suture Anchors: Technique, Technology, and Pitfalls. *Clin. Orthop. Relat. Res.* 17–30 (2001).

81. Elder, M. *ADVANCED ORTHOPEDIC TECHNOLOGIES, IMPLANTS AND REGENERATIVE PRODUCTS*. **7215,** (2014).

82. Timoney, P. J., Krakauer, M., Wilkes, B. N., Lee, H. B. H. & Nunery, W. R. Nylon foil (supramid) orbital implants in pediatric orbital fracture repair. *Ophthal. Plast. Reconstr. Surg.* **30,** 212–4 (2014).

83. ATEX Technologies Inc. MEDICAL APPLICATIONS. (2013). at <http://www.atextechnologies.com>

84. Textile Development Associates, I. Surgical Mesh & Felt for Medical Device Manufacturers. (2014).

85. Wellesley, W. S. *MARKET RESEARCH REPORT ADVANCED ORTHOPEDIC TECHNOLOGIES , Melissa Elder*. **7215,**

86. Sullivan, F. &. *U. S. Moist Wound Dressings Market*. (2002).

87. Elder, M. *Markets for Advanced Wound Management Technologies*. **7215,** (2014).

Curriculum Vitae

400 N Broadway, Smith 5001C, Baltimore, MD, USA 21287 ◆ 443-854-2070 ◆ ccook32@jhu.edu

Education:

PhD Candidate in Medical Engineering, California Institute of Technology 2014-2020

Master of Science in Engineering, Johns Hopkins University 2012-2014

- CGPA of 4.0 in biomedical engineering
- Executive of the Biomedical Engineering Masters Student Council
- Position in the Grayson Lab for Craniofacial and Orthopedic Tissue Engineering

Bachelor of Applied Science in Engineering Science, University of Toronto 2008-2012

- Major in biomedical engineering
- 90 percent CGPA, pass with honors

Ontario Secondary School Diploma, Ridgeway Crystal Beach High School 2004-2008

- Graduated with a 99.7 percent average
- Governor General's Medal and Excellence in Education Award

Awards and Scholarships

- Alexander Graham Bell Canada Graduate Scholarship (CGS M), 2012
  Awarded to top-ranked NSERC applicants in master's programs in natural sciences or engineering
- C.D. Howe Memorial Foundation Engineering Scholarship, 2009-2012
  $22500 over 3 years to national recipient, for outstanding academic achievement in engineering
- The Award of Excellence, 2012
  In recognition of academic excellence (top ~2%) by the Division of Engineering Science, U of T
- Summer Undergraduate Studentship, 2011
  Top summer research student in Department of Medical Biophysics, Faculty of Medicine, U of T
- Shaw Design Scholarship, New College Scholarship, 2010
  For outstanding engineering design and academic achievement, respectively
- Other merit-based scholarships and awards covering undergraduate tuition

Research-Related Experience:

Masters Thesis Sept 2012-2014

Supervised by Dr Warren Grayson, Johns Hopkins University, MD, USA

- Designed and built a bioreactor for the culture of 3D fibers capable of applying axial strain, monitoring real-time contractions and fiber stiffness, as well as calculating 3D strain fields experienced by the cells
- Invented a technology capable of sustained delivery of oxygen to cells in tissue engineered grafts to mitigate the negative effects hypoxia
- Supervise the research projects of two undergraduate students within the lab

Undergraduate Thesis **Sept 2011-May 2012**

Supervised by Dr. John Rubinstein, University of Toronto, Canada

- Investigated the structural mechanism preventing proton translocation through the V_o membrane region in dissociated yeast v-ATPase by cryo-EM methods
- Purification of V_o, optimization of sample conditions for cryo grids, acquisition of single particle images by cryo-electron microscopy, particle selection, construction of class averages, 3D model construction
- Results tentatively indicate a novel control mechanism whereby the arm of the a-subunit interacts with the d-subunit, immobilizing the membrane-bound c-ring and preventing proton translocation; further investigation will be required to fully validate these results

Summer Research in Molecular Structure and Function **May-Sept, 2011**

Supervised by Dr. John Rubinstein, The Hospital for Sick Children, Toronto, Canada

- Investigated the putative calmodulin induced homodimerization of V_o membrane bound region of yeast v-ATPase, with interest in structural characterization
- Work involved genetic tagging of V_o region, cell culture, optimization of purification protocol for V_o, various chromatography techniques for purification and characterization (affinity, ion exchange, size-exclusion, etc.), construction of a fluorescent 6xHis tagged yeast calmodulin, characterization by negative stain electron microscopy, mass spectrometry, binding assays, etc.

Laboratory-Based Course Work **2010-2011**

BME 340 Biomedical Engineering Techniques and BME496 Cellular Bioengineering

- Courses devoted to practical lab experience with relevant biomedical lab techniques: cell culturing including stem cells, microscopy, ELISA, PCR/Electrophoresis, transfection, quantitative immunostaining, micro-patterning, cryo-preservation, computer modeling, etc.

Summer Research in Nanomaterials and Renewable Energy **May-August, 2009**

Supervised by Dr. Ho Ghim Wei, National University of Singapore, Singapore

- Investigated the application of nanomaterials to dye-sensitized solar cells
- Developed laboratory techniques and familiarity with scanning electron microscopy, X-ray crystallography, and other characterization techniques
- Constructed a novel 6.4% efficient cell, setting a record within the research group
- Optimized and created synthesis routes for varying sized nanoparticles of TiO_2
- Contributed work for the publication of a paper in the Journal of Power Sources

Publications:

Yilgor Huri P, **Cook C.A.**, Hutton DL, Goh BC, Gimble JM, Digirolamo DJ, Grayson WL. (2013) Biophysical cues enhance myogenesis of human adipose derived stem/stromal cells. Biochem Biophys Res Commun. 438(1):180-5.

Yilgor Huri P, Temple JP, Hung BP, **Cook C.A.**, Grayson WL, (Eds: Ajaykumar Vishwakarma, Paul Sharpe, Songtao Shi, Xiu-Ping Wang and Murugan Ramalingam). (2013) Bioreactor Technology for Engineering Craniofacial Tissues, in Stem Cell Biology and Tissue Engineering in Dental Science.

Agarwala, S., Thummalakunta, L. N. S. a. N. S. A., **Cook C.A.**, Peh, C. K. N. K. N., Wong, a. S. W. S. W., Ke, L., & Ho, G. W. W. (2011) Co-existence of LiI and KI in filler-free, quasi-solid-state electrolyte for efficient and stable dye-sensitized solar cell. Journal of Power Sources. 196(3), 1651–1656.

Patents:

Cook, C.A. (Primary Inventor), Grayson, W. (2013) Controlled Outgassing of Hyberbarically Loaded Materials for the Delivery of Oxygen and Other Therapeutic Gases in Biomedical Applications. Full provisional patent, #US 61,828,126.

Grayson, W. (Primary Inventor), Huri, P., Hutton, D., **Cook, C.A.**, Temple, J. (2013); Bone Regeneration Using Stromal Vascular Fraction, Platelet-Derived Growth Factor-Rich Hydrogel, Three- Dimensional Printed Poly-E-Caprolactone Scaffolds. Full provisional patent, #US 61,828,114.

Other Experience:

- Teaching assistant for Praxis I & II, first-year courses in engineering design
- Student representative to meet with special visiting committee for the dean of engineering's application for NSERC Chair in Multidisciplinary Engineering Design
- Work experience in custom manufacturing, machining, microfabrication

References

Available on request